Characterizing Subsurface Structural Features of the Bellingham Basin by Gravity and Magnetic Modeling

by

Rahul Bhattacharya

A thesis submitted to the Graduate Faculty of

Auburn University

In partial fulfillment of the requirement for the Degree of

Master of Science

Auburn, Alabama

December 14, 2019

Approved by

Lorraine W. Wolf, Chair, Professor of Geophysics

Mark G. Steltenpohl, Professor of Geology

Haibo Zou, Professor of Geology

Abstract

This study uses gravity and magnetic data modeling to identify the geometry of the Bellingham basin, Washington, and its deformational history. The study also provides additional insight into three newly identified Holocene-active faults, Drayton Harbor, Birch Bay, and Sandy Point, that are linked with ongoing basin deformation.

The models resulting from this analysis show the Bellingham basin as an arcuate-shaped, east-west-trending basin. The extent of the basin to the west is not revealed owing to a lack of offshore data. The Cascade Mountains form the basin's eastern boundary. On the east side of the basin, the Boulder Creek fault forms the basin's northern boundary, which may have been reactivated by ongoing crustal block rotation. Wavelength filtering of magnetic field data show distinct magnetic lineations, or "contacts," that are assumed to result from juxtaposed rock units. Several of the contacts align with the Drayton Harbor, Birch Bay and Sandy Point faults, and suggest that the faults continue into the basin. Based on cross-sectional modeling and the filtered maps, the study postulates minimum lengths of 30, 30, and 24 km for the Drayton Harbor, Birch Bay, and Sandy Point faults, respectively. In this study, the Sandy Point and Birch Bay faults have been modeled as reverse faults with the northern side up. Drayton Harbor, although mapped as south-side up in previous work along the western shoreline, does not exhibit significant offset in its projected position onto the cross-sectional models. This result suggests that the Drayton Harbor fault does not extend far

into the basin, or alternatively, the sense of slip along the fault is predominantly strike-slip as it continues into the basin.

Epicenters of recorded earthquakes in the Bellingham basin appear closely aligned with the Birch Bay and Sandy Point faults, supporting the idea that these faults are currently active. Similarly, the moderately large (M = 5.0) 1990 Deming, WA, earthquake, which occurred ~ 7 km south of the Boulder Creek fault, along with scattered seismicity throughout the deep basin, provides evidence of ongoing deformation related to crustal block rotation and north-south directed compression. Results from this study and previous work argue that these crustal faults within the Bellingham basin should be considered in assessing seismic hazard in the Puget Sound region.

Acknowledgments

I would like to thank my advisor Dr. Lorraine Wolf for her guidance and help in this project. The challenges in this project were easy to overcome because of her constant direction and support. I would also like to thank my committee members Dr. Mark Steltenpohl and Dr. Haibo Zou for their valuable suggestions and insights in this work. I appreciate the Geosciences Advisory board for providing financial support in this project. I would also like to thank Auburn University College of Science and Mathematics (COSAM) for providing travel support to present my research results at the Symposium on the Application of Environmental and Engineering Geophysics (SAGEEP) 2019, Portland.

I am thankful to Richard Blakely for providing the gravity data used in this study. I would also like to thank M. Anderson and J. Taylor for additional gravity data collection and their processing that improved the database. I appreciate Dr. Stephanie Rogers for helping me in exploring the ArcGIS database for the Pacific Northwest. Furthermore, I am grateful to USGS for supporting the gravity data collection by USGS NEHRP grant (USGS-G11AP20042) to Dr. L. Wolf. Also, this work would not be easily accomplished without the help of the Geosoft Oasis Montaj™ technical support division.

Finally, I would like to thank my family for their constant support and motivations.

Table of Contents

List of Tables

List of Figures

List of Abbreviations

GPS	Global Positioning System
CBA	Complete Bouguer Anomaly
TFA	Total Field Anomaly
QS	Quaternary sediments
CN	Chuckanut formation
EA	Easton metamorphic suite
BP	Bell Pass mélange
CH	Chilliwack group
YA	Yellow Aster Complex
BB	Birch Bay fault
DH	Drayton Harbor fault
SP	Sandy Point fault
VM	Vedder Mountain fault
BCF	Boulder Creek fault
PNSN	Pacific Northwest Seismic Network

Introduction

The subduction of the Juan De Fuca plate beneath the North American plate in the Pacific Northwest occurs at a rate of ~ 50 mm/yr (Demets et al., 1994) and results in an active convergent margin known as Cascadia forearc. Global Positioning System (GPS) studies show clockwise rotation and north-south compression of crustal blocks within the North American plate (McCaffrey et al., 2013). Locally, northward migration of the Oregon Coast block is producing compression of western Washington against the stable Canadian buttress (Figure 1a) (Wells et al., 1998; McCaffrey et al., 2013). Deformation resulting from these complex plate interactions and block rotations are accommodated by a series of folds and faults that define forearc basin boundaries and control basin evolution over time. Major forearc basins in this region from the south to north are the Tacoma basin, Seattle basin, Everett basin, and Bellingham basin (Figure 1b). Faults within and outside of these forearc basins have been active during the Holocene Period, making them useful for assessing the earthquake hazard in this region. Examples of moderate to large magnitude earthquake events triggered by Holocene-active faults are as follows: the ~A.D. 900-930 M ~ 7 earthquake, thought to have occurred on Seattle fault zone (Atwater et al., 2003; Bucknam et al., 1992; Satake et al., 1996); the 1965 Puget sound intraslab earthquake (M 6.7); and the 2001 Nisqually intraslab earthquake (M 6.8) (Ichinose et al., 2004).

Within the Bellingham basin, most recent seismicity is of low magnitude (M < 3); however, faults within the basin are capable of generating larger magnitude earthquakes (e.g., 1990, M=5.0 Deming earthquake Figure 2). Many of the crustal faults are concealed, at least partially, by the thick sedimentary cover within the basins or dense forest canopy, making

them difficult to identify using surface geological mapping (Pratt et al., 1995). Lack of surface exposure or access has encouraged the use of geophysical techniques for understanding the earthquake hazard in the Cascadia subduction zone and for mapping potential seismic sources in the upper crust. In addition to earthquake and active source seismology, potential methods such as gravity and magnetic data have yielded helpful information to constrain the location and geometry of Holocene-active faults in the upper plate (e.g., Finn, 1990; Blakely, 1999).

To improve the understanding of upper-plate deformation, this study uses gravity and magnetic data to investigate the crustal structure and possible seismic sources in the Bellingham basin, the northernmost forearc basin (Figure 1b). The study incorporates anomaly mapping and wavelength-filtering techniques to identify the shallow subsurface deformation. To gain knowledge of subsurface relationships, the study includes 2.5D forward modeling of two cross-sectional profiles that are positioned to cross major geologic features. This study expands upon and carries forward the findings of Taylor (2013), whose preliminary analysis supported the hypothesis that at least two Holocene-active faults extend into the Bellingham basin. The goal of this study is to refine the model proposed by Taylor (2013) for the crustal structure of the Bellingham basin. Specifically, it seeks to address the following questions:

(1) What is the geometry and deformation history of the Bellingham basin?

(2) Do Holocene-active faults discovered along the shoreline of western Washington extend into the Bellingham basin?

(3) What is the configuration and extent of faults within the basin?

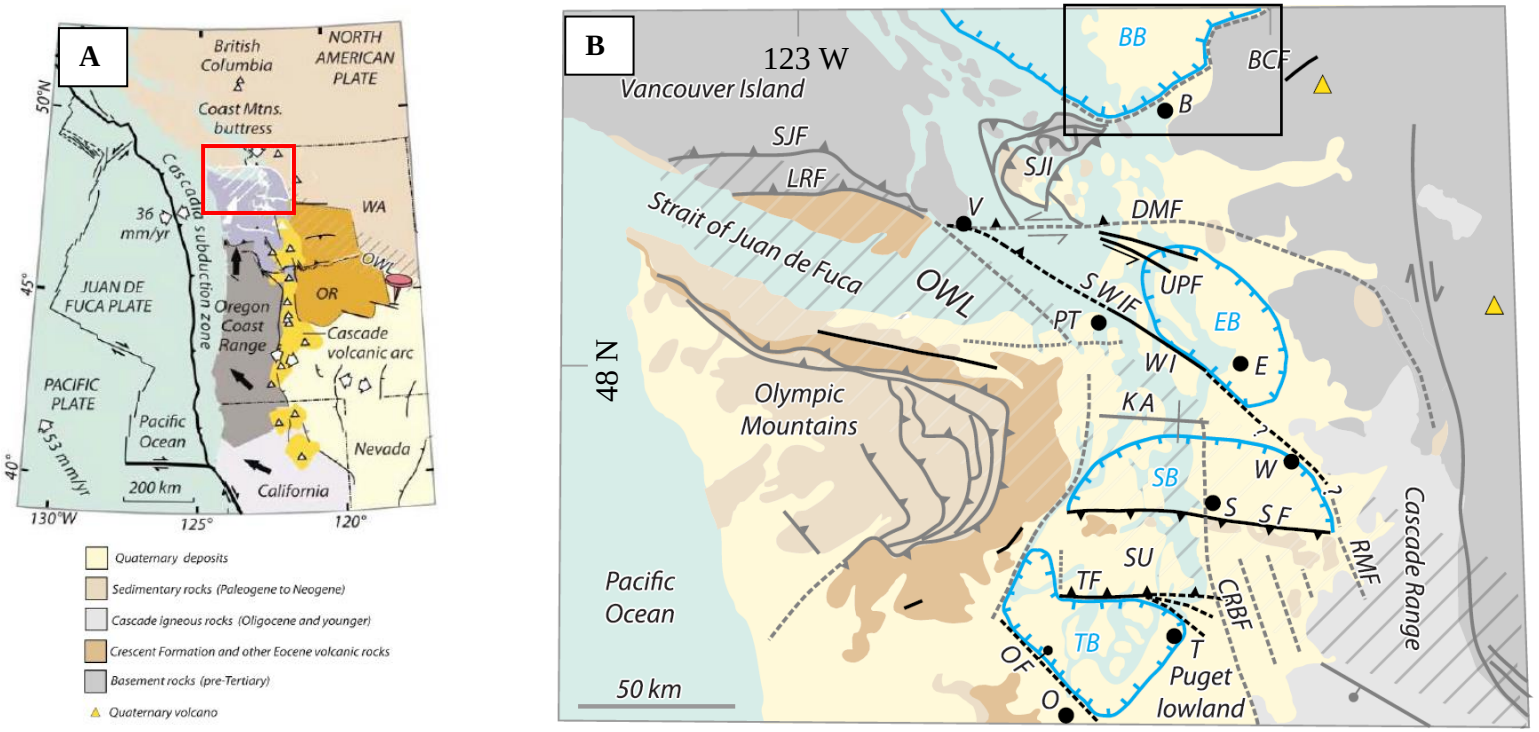

Figure 1. A: Tectonic map of the study area (red rectangular outline) showing relative motion of crustal blocks in the Cascadia forearc (Sherrod et al., 2008; Wells et al., 1998). The study area is situated between the northward-migrating Oregon coast block and a stationary Canadian buttress. Red pin=pole of rotation for crustal blocks in the forearc (McCaffrey et al., 2013). B: Northern Cascadia major faults (Sherrod et al., 2008): OF= Olympia fault; TF= Tacoma fault; SF= Seattle fault; SWIF= Southern Whidbey Island fault; UPF= Utsalady Point fault; DMF= Devils Mountain fault; BCF= Boulder Creek fault; (Kelsey et al., 2012; Wells et al., 1998). Blue polygons (with inward hatched lines) indicate sedimentary basins: TB= Tacoma basin; SB= Seattle basin, EB= Everett basin, and BB= Bellingham basin. Other abbreviations as in Sherrod et al., 2008.

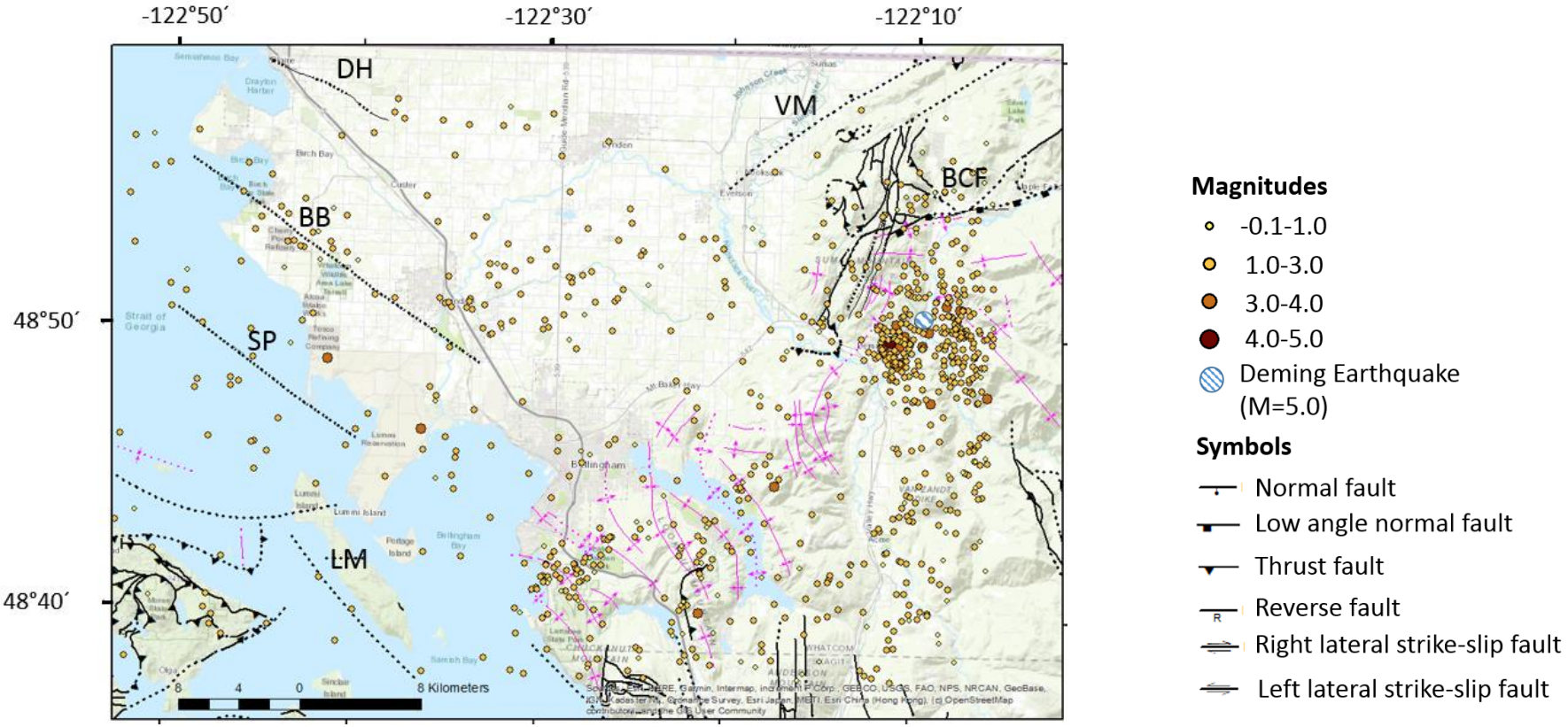

Figure 2. Earthquakes in the Pacific Northwest (1969-present). The relative sizes of the circles represent relative magnitude of earthquakes (up to magnitude 5.0) from PNSN Events | Pacific Northwest Seismic Network (https://pnsn.org/events?custom_search=true; last accessed: July, 2019). Black lines= faults (dotted where inferred) from Geology GIS Data and Databases | WA – DNR (https://www.dnr.wa.gov/programs-and-services/geology/publications-and-data/gis-data-and-databases; last accessed: July, 2019). Abbreviations: DH= Drayton Harbor fault; BB= Birch Bay fault; and SP= Sandy Point fault; VM= Vedder Mountain fault; BCF= Boulder Creek fault; LM= Lummi island.

Geologic Setting

The Cascadia forearc is a complex tectonic setting resulting from subduction of the Juan De Fuca plate beneath the North American plate (Figure 1). Ongoing deformation is evidenced by seismicity and data from global positioning surveys (GPS) (Figures 1 and 2) (McCaffrey et al., 2013). In the northern part of this forearc, the northward migration of the Oregon Coast block is compressing western Washington against a stable Canadian buttress, resulting in a north-south-oriented stress field and a crustal shortening of 4.5mm/yr (Mazzotti et al., 2002; McCaffrey et al., 2013). This crustal shortening is accommodated by upper crustal deformation in the form of folds and faults that separate a series of forearc basins (i.e., Tacoma basin, Seattle basin, Everett basin, and Bellingham basin). The major faults separating these basins are the Olympia fault (Sherrod, 2001), the Tacoma fault (Sherrod et al., 2000), the Seattle fault (Bucknam et al., 1992; Sherrod et al., 2000; Blakely et al., 2002; Nelson et al., 2003; Brocher et al.; 2004; Kelsey et al., 2004), the Southern Whidbey Island fault (Johnson et al., 1996; Kelsey et al., 2004; Sherrod et al., 2005), and the Devil's Mountain fault (Johnson et al., 2001). Several other faults, such as the Utsalady Point fault (Johnson et al., 2004), the Boulder Creek fault (Haugerud et al., 2005; Barnett et al., 2006), the Sandy Point fault (Kelsey et al., 2012; Polivka, 2013), the Birch Bay fault (Kelsey et al., 2012; Polivka, 2013), and the Drayton Harbor fault (Kelsey et al., 2012), appear to cut through the basins. The extent of these faults, however, is obscured by thick sequences of sediments overlying the forearc basins (Easterbrook, 1976).

This study is focused on the Bellingham basin, the northernmost basin in the Cascadia active margin. Development of the Bellingham basin is thought to have begun in the mid-Tertiary. It has been continuously modified by the adjacent volcanic arc and by deposition of glacial deposits and alluvial sediments eroded from the Cascade Mountains to the east (Booth, 1994; Kelsey et al., 2012). The evolution of Bellingham basin is debated but the existence of the Boulder Creek fault at the northeastern margin (Barnett et al., 2006) indicates that this basin had been developed by the north-south strain resulting from forearc compression. The stratigraphy of this basin can be divided into six major rock units (Table 1). From oldest to youngest these rock units are the Yellow Aster Complex, the Chilliwack Group, the Bell Pass Mélange, the Easton Metamorphic Suite, the Chuckanut Formation, and Quaternary sediments (Brown and Dragovich, 2003). The youngest layer, Quaternary sediments (QS), consists of glacial and alluvial sedimentary rocks. The protoliths of these rocks are varied types of igneous, sedimentary, and metamorphic rocks. Below this layer is the Chuckanut Formation (CN), consisting of alluvial deposits of sandstones, siltstones, conglomerates and coal. The tectonic setting of these rocks were intracontinental rift zones (Gresens et al., 1981). The Chuckanut Formation overlies Easton Metamorphic Suite (EA), which consists of carbonaceous phyllites, metagraywackes, metabasites, siliceous carbonaceous phyllites, meta-peridotite, gabbro-tonalite plutons, and metatuffs. These rocks were deposited in an ocean ridge or trench settings (Misch, 1966; Brown, 1986). Below the EA, another layer, known as Bell Pass Mélange (BP), consists of assemblages of chert, oceanic basalt, and volcanic lithic clastic rocks supported by less competent sedimentary rocks (Blackwell, 1983). Some of these rocks are accreted exotic rocks along with rocks deposited in a trench setting (Misch, 1966; Brown, 1987). Below the BP layer, the Chilliwack Group (CH) consists of a varied composition of volcanic lithic sandstone, siltstone, fossiliferous limestones, and basaltic to dacitic volcanic rocks. These rocks were deposited in

an island arc setting. The oldest unit, inferred to be the Yellow Aster Complex (YA), consists of rocks derived from siliceous garnet-pyroxene gneiss, calc-silicates, marble, gabbro-tonalite plutonic rocks and basalt-andesite hypabassal rocks. (Misch, 1966). This formation was deposited in a passive continental margin setting.

Brown and Dragovich (2003) provide one of the few comprehensive geologic maps of the Bellingham basin and surrounding area of western Washington (Figure 3). They prepared three cross-sections from this map, one of which is close to the study area and covers the southern part of the Bellingham basin (line B-B', Figure 4). The rock units shown in this cross-section are analogous to those described above. The cross-section B-B' indicates three major faults but no faulting near to the Bellingham basin's southern extent. The displacement and deformation in the cross-section indicate the faults have been active during the Holocene time.

Table 1. Geologic units and tectonic units of the study area from Brown and Dragovich (2003) and Taylor (2013).

Unit	**Time Interval**	**Tectonic Setting**	**Protolith**
Glacial Sediments	Quaternary	Sedimentary basin (fluvial)	Previously deposited units of all types (Igneous, sedimentary, and metamorphic)
Chuckanut Formation	Tertiary (Eocene-Oligocene)	Intracontinental rift zones, likely strike-slip pull apart basins	Arkosic and lithic sandstone, siltstone, conglomerate, and coal. Mostly fluvial with some marine deposits.
Easton Metamorphic Suite	Jurassic	Ocean ridge, trench, transitional area to island arc	Metabasite, siliceous carbonaceous phyllite, metagrawacke, metabasalts, gabbro-tonalite plutons, and Metatuffs.
Bell Pass Mélange/ Orcas Chert	Triassic-Middle Jurassic	Ocean floor and trench with some exotic accreted rocks	Ribbon chert, mudstone, pillow basalt, limestone, volcanic lithic clastic rocks.
Chilliwack Group/East Sound Group	Devonian-Permian	Island arc	Volcanic lithic sandstone, siltstone, basaltic to dacitic volcanic rocks, andesitic to dacitic rocks, fossiliferous to reefoidal limestone, shale, argillite, graywacke, and conglomerate
Young Aster Complex	Pre Devonian to Devonian	Passive continental rift margin	Siliceous garnet-pyroxene gneiss, calc-silicates, marble, gabbro-tonalite plutonic rocks, and basalt andesites.

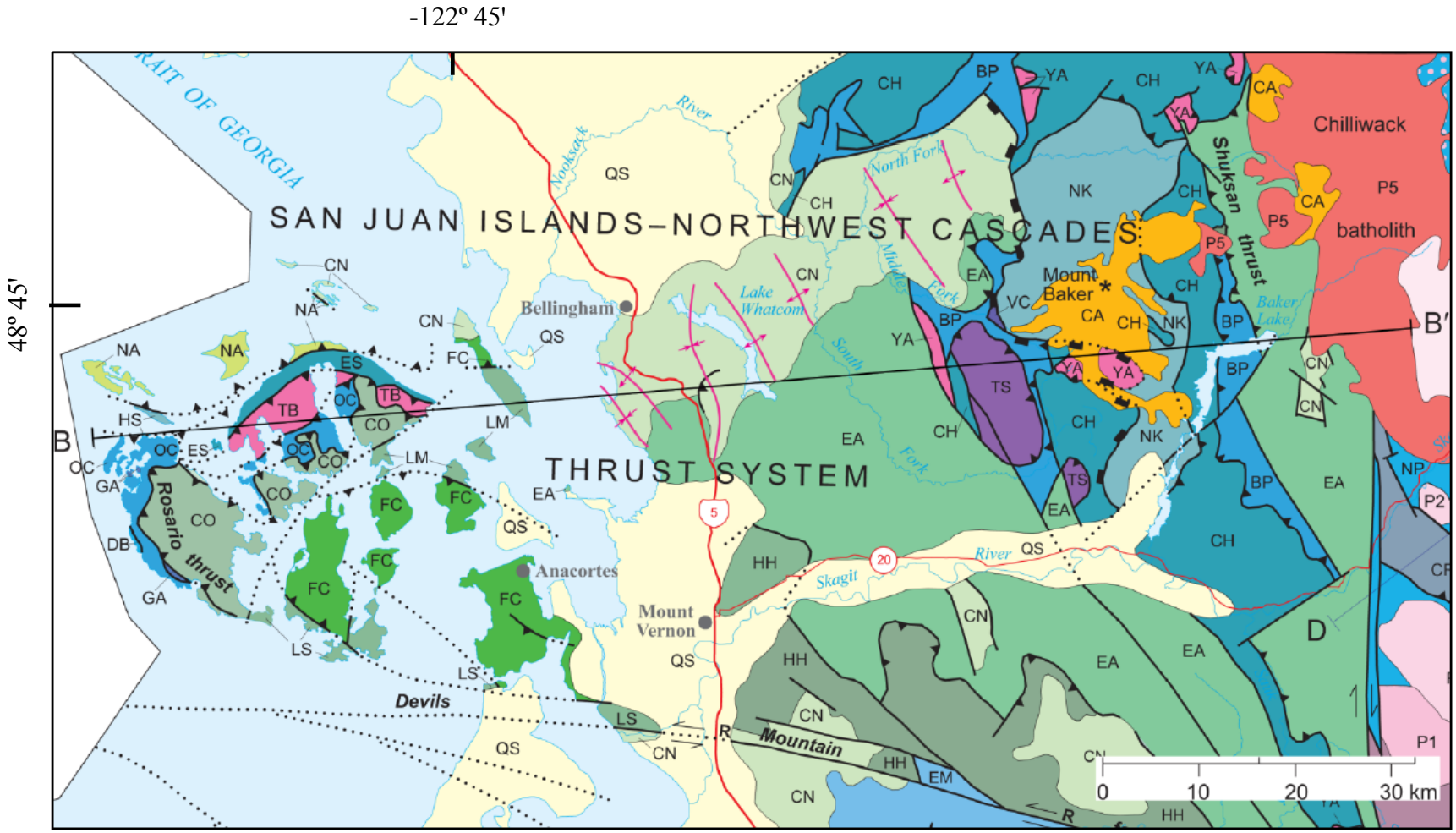

Figure 3. Geologic map of the Bellingham study area modified from Brown and Dragovich (2003). Line B-B′ shows the location of a geologic cross-section. Solid black lines indicate contacts (depositional or intrusive). Dotted lines indicate concealed faults. Magenta lines with arrows represent anticlines and synclines. Other abbreviations represent units and structures as listed in Brown and Dragovich (2003).

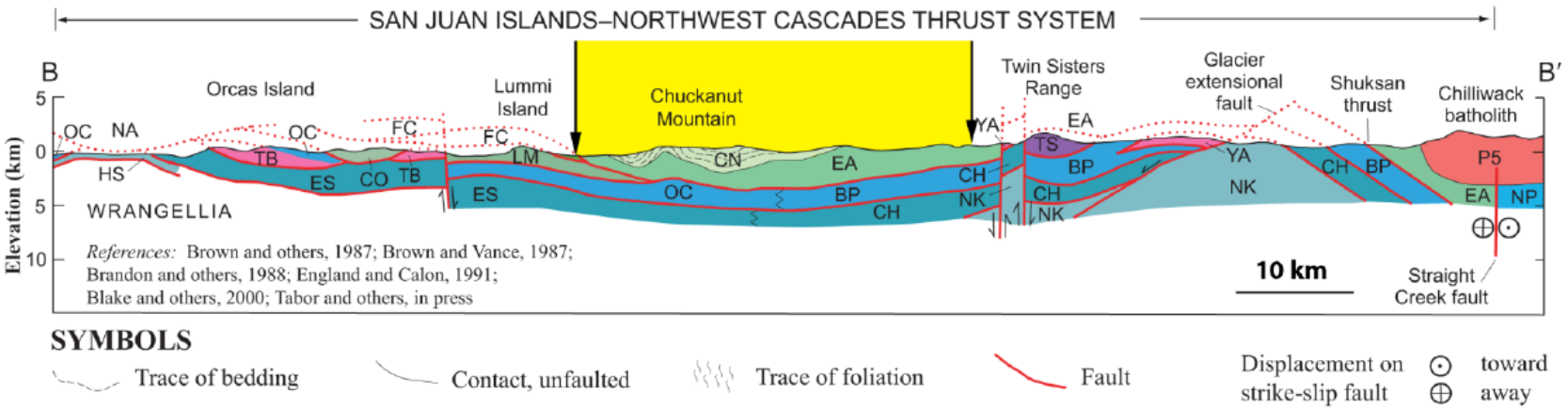

Figure 4. Geologic cross-section (west to east) of line B-B′ (Figure 3) from Brown and Dragovich (2003). The yellow region, bounded by vertical arrows, represents the location of the Bellingham basin. Abbreviations: CN=Chuckanut Formation; EA= Easton Metamorphic Suite; OC=Orcas Chert; BP=Bell Pass Mélange; ES=East Sound Group; CN=Chilliwack Group; YA= Yellow Aster Complex. Other abbreviations represent units and structures as listed in Brown and Dragovich (2003).

Previous Studies

Light Detection and Ranging (LiDAR) data (Kelsey et al., 2012; Haugerud et al., 2013) and seismic reflection imaging (Pratt et al., 1997) have been used to understand subsurface deformation in the Puget Sound area. In their study of the Bellingham basin, Kelsey et al. (2012) provided evidence of Holocene faulting in the basin based on the radiometric dating of wood and seed samples from shallow cores taken along the northern and southern segments of the Birch Bay fault. Samples from these cores indicate a reverse sense of motion along the Birch Bay fault, with the northern side up (Figure 5). Previous seismic reflection imaging by American Hunter Exploration Ltd (Hurst, 1991) supports this fault geometry, associating the fault with the crest of an anticlinal fold (Figure 6). LiDAR imaging and magnetic lineament studies (Kelsey et al., 2012) also yielded information on two other faults within the Bellingham basin: the Drayton Harbor and Sandy Point faults to the north and south of the Birch Bay fault, respectively (Figure 3). According to their results, Kelsey et al. (2012) claims that the Sandy Point fault has a similar offset to that of the Birch Bay fault, but the Drayton Harbor fault indicates the opposite sense of motion. Interpretation of offshore seismic imaging done by Western Geophysical identified the presence and mechanics of both Sandy Point and Birch Bay faults farther to the west (Figure 7) (Polivka, 2013). Polivka (2013), however, identified the Birch Bay fault as a dextral fault, with the Birch Bay and Sandy Point faults connected by a regional decollement.

Other than these studies, additional information about the faults within the Bellingham basin was provided by a gravity survey conducted by Taylor (2013). In his study, Taylor (2013) added approximately 160 new measurements to an existing U.S. Geological Survey (USGS) database. His analysis, which was based on both the newly compiled gravity data set and previously acquired aeromagnetic data, included two cross-sectional models across the Bellingham basin, one along a north-south profile and the other from southwest to northeast (Figures 8 and 9). In addition, he used wavelength-separation methods in an attempt to map the basin geometry and several crustal faults. His results suggest that the Bellingham basin as an arcuate-shaped basin significantly smaller in extent than previously defined (e.g., Gallup, 1957; Kelsey et al., 2012), especially towards the western flank of the basin. The results also suggest that although the Birch Bay and Drayton Harbor faults continue for some distance into the basin, their full extent is unknown. Although Taylor's results are consistent with the previous results of Hurst (1991) and Kelsey et al. (2012), they do not unequivocally resolve questions on the basin evolution and its existing active structures. In addition, the profiles modeled in the previous study are not positioned well for characterizing the Sandy Point fault and its relationship to the basin geometry.

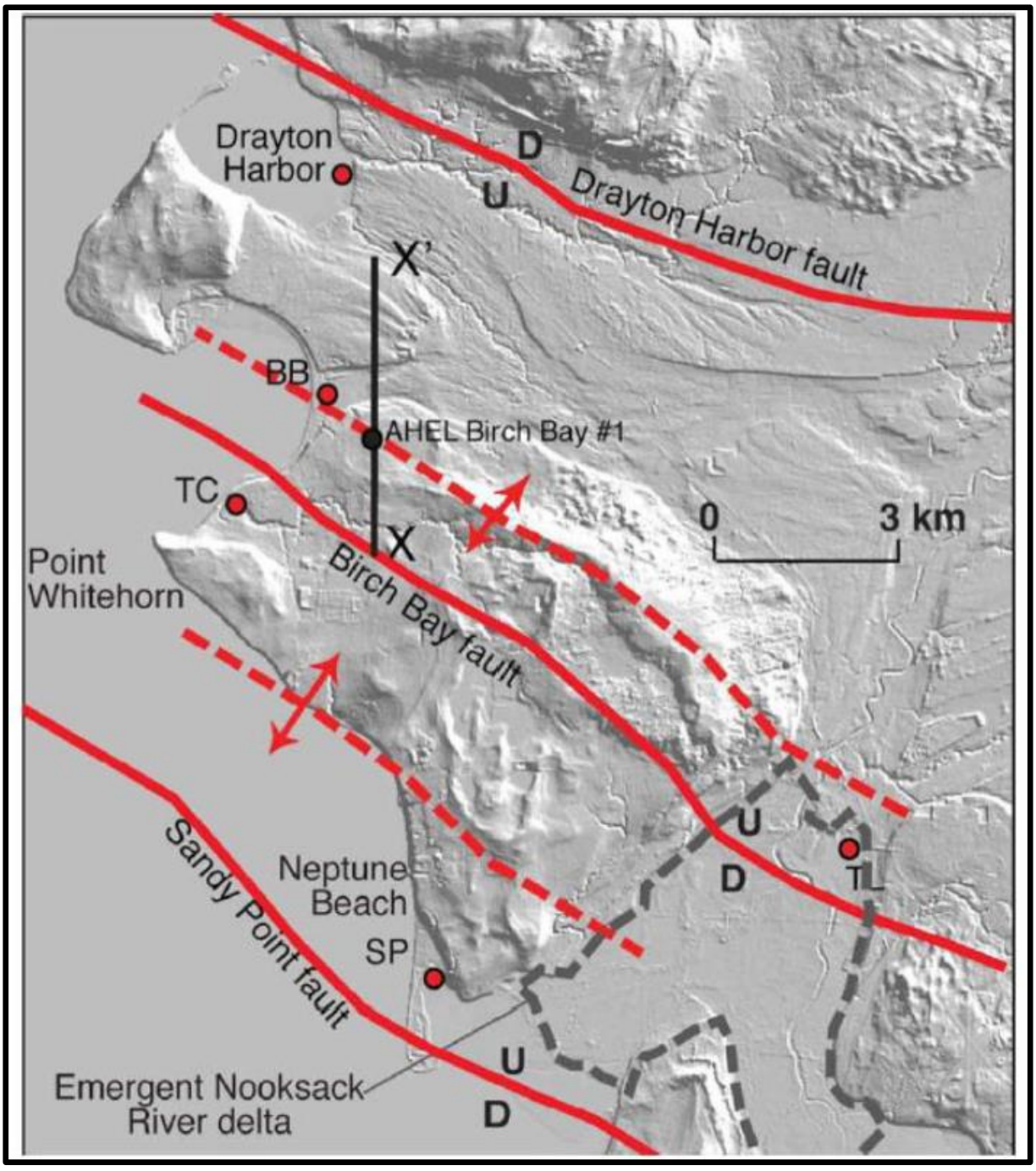

Figure 5. LiDAR Digital Elevation Model (DEM) collected by USGS with faults (solid red lines) and anticlines (red dashed lines) superimposed. Faults correspond to lineaments seen in aeromagnetic data (Kelsey et al., 2012). Red dots indicate paleoseismic study sites. Gray dashed lines indicate location of the Nooksack river delta. Also shown is the location of seismic reflection line (X-X') acquired by American Hunter Exploration Ltd. (Hurst, 1991).

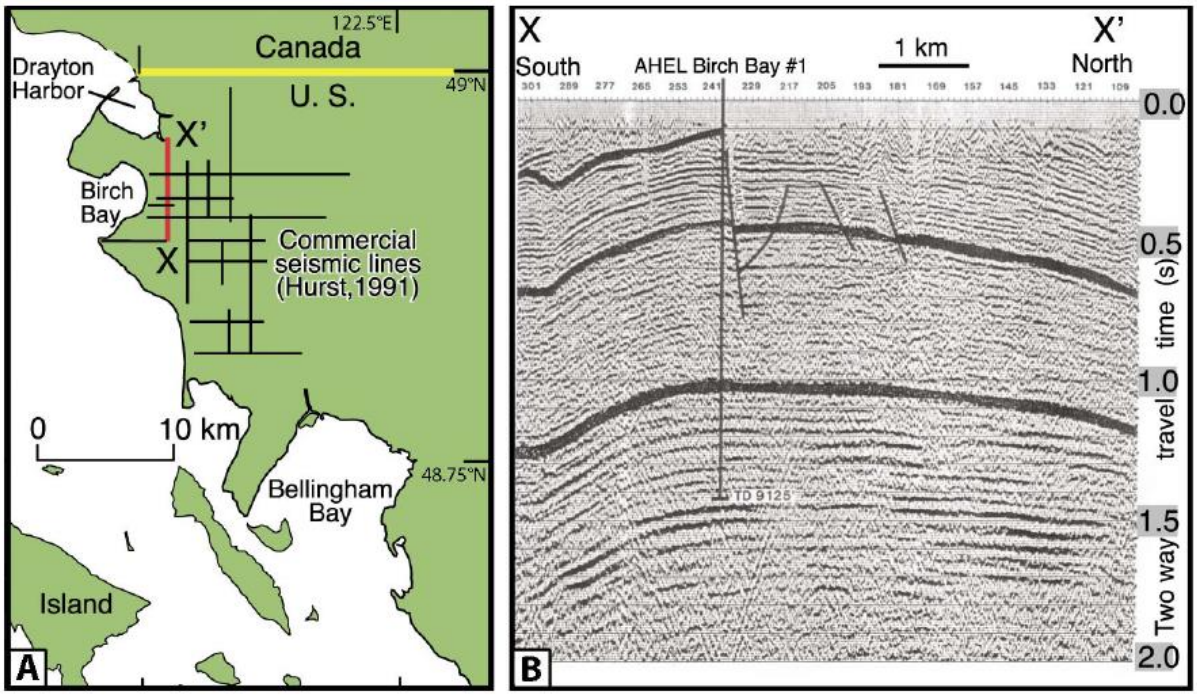

Figure 6. Left: Regional map of the study area with the commercial seismic lines' orientation (Hurst, 1991). X-X'= Seismic line done by American Hunter Exploration Ltd.
Right: Seismic line X-X' with the location of the stratigraphic well AHEL Birch Bay #1 (Kelsey et al., 2012).

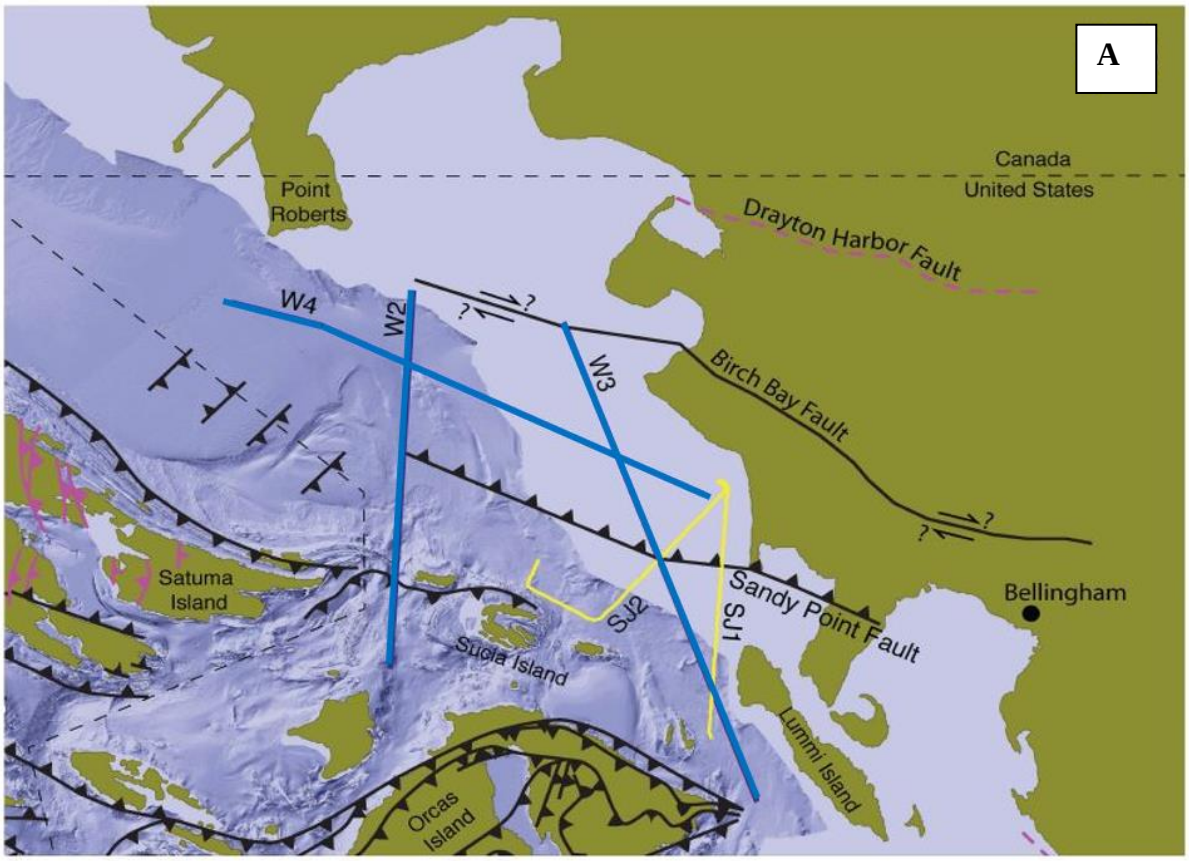

Figure 7. A: Inferred fault movements offshore of the study area with marine seismic survey line locations superimposed (Polivka, 2013). Blue lines (W3, W2, and W4) =marine seismic survey done by Western Geophysical. Yellow lines (SJ1 and SJ2) =Centennial sparker survey lines. Black lines=faults; Thrust faults have teeth on upthrown block. Dashed pink line=possible fault trace of the Drayton Harbor fault.

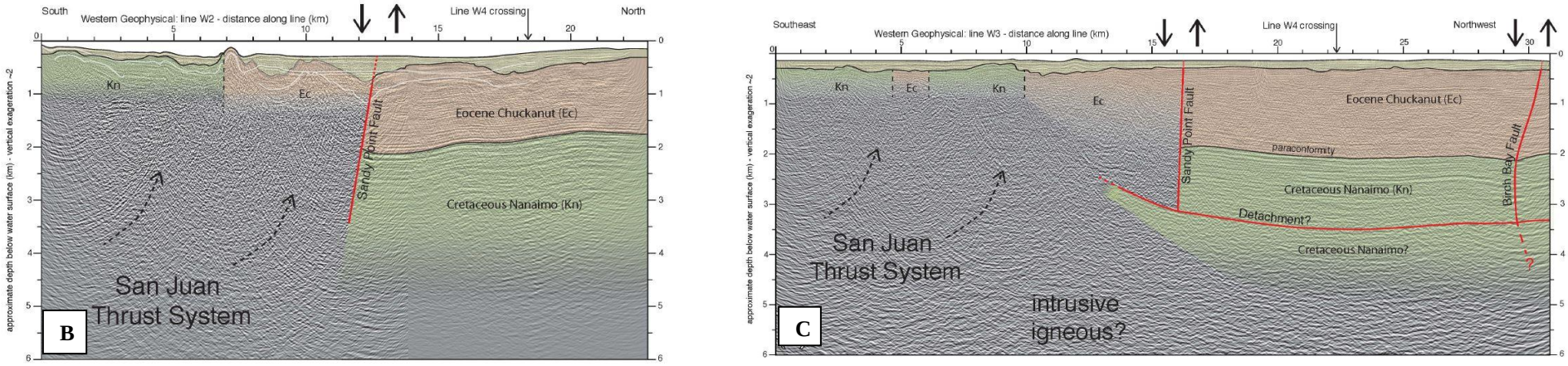

Figure 7 (con't). B: Interpretation of the offshore Western Geophysical seismic survey line W2 (Polivka, 2013). C: Interpretation of the offshore Western Geophysical seismic survey line W3 (Polivka, 2013). Red lines=faults. Black dashed lines=San Juan thrust system. Reflectors south of the Sandy Point fault lack coherency, possibly due to over-migration, igneous intrusions, contact metamorphism, and/or highly metamorphosed rocks near Lummi Island. White lines are multiples. Abbreviations: Ec=Eocene Chuckanut Formation; Kn=Cretaceous Nainamo Formation. According to Polivka (2013), the geometry of the Birch Bay fault indicates growth faulting because of the increase of reflectors dip with depth. His model shows both the Sandy Point and Birch Bay faults sole to a detachment.

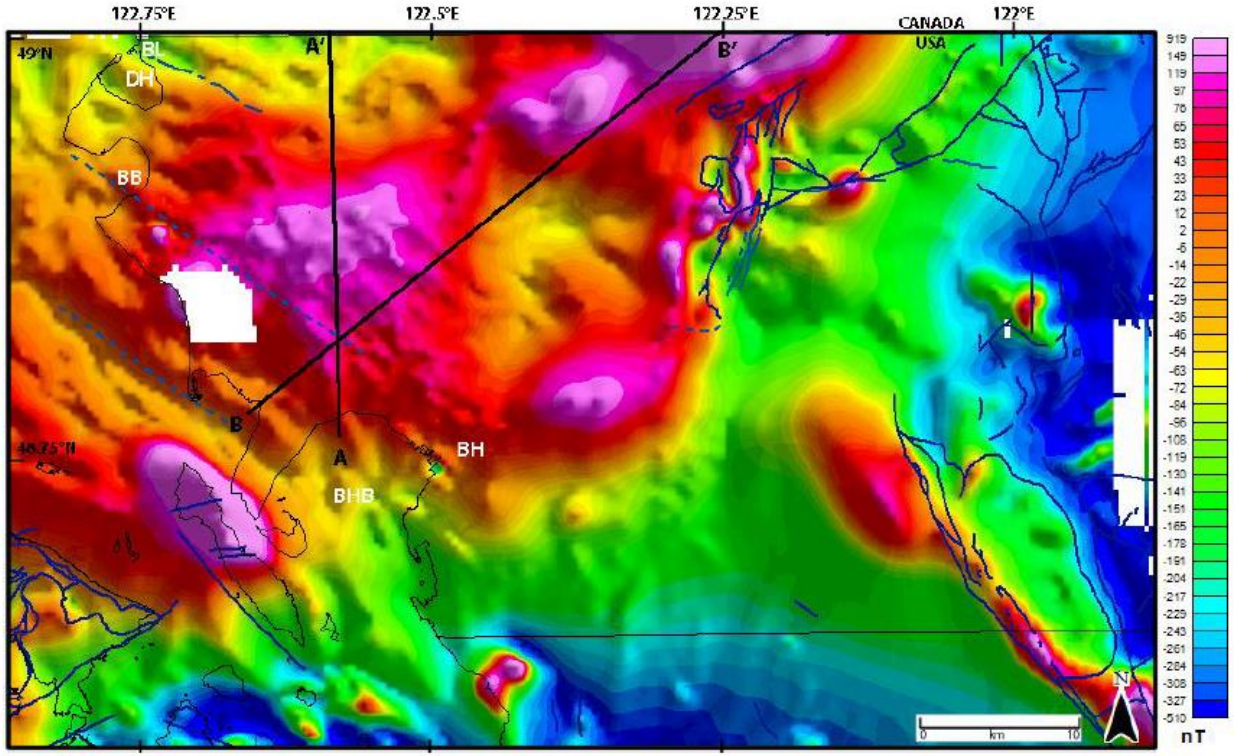

Figure 8. Total field anomaly (TFA) map of the Bellingham basin area by Taylor (2013). Solid blue lines=mapped faults. Dashed blue lines=inferred faults, White polygon=masked area due to smelter operation. Black lines=locations of cross-sectional profile A-A' and B-B' of Taylor (2013). Abbreviations: BHB= Bellingham bay; BH= Bellingham basin; DH=Drayton Harbor fault; BB=Birch Bay fault.

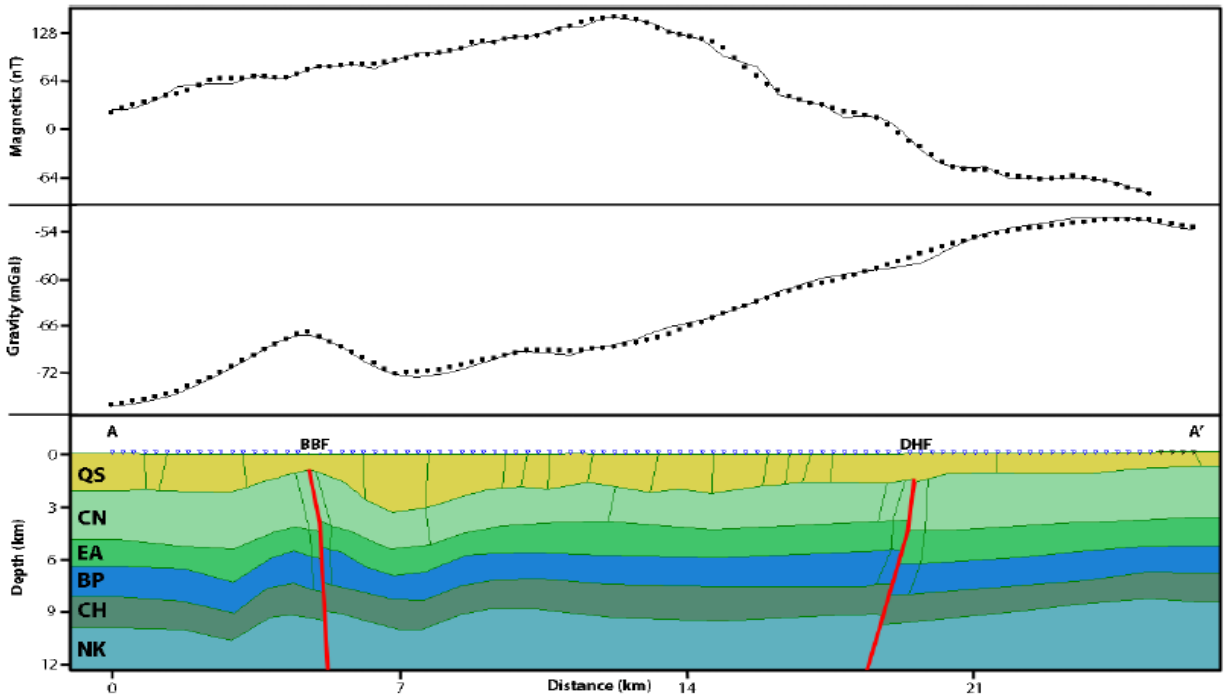

Figure 9. Calculated and observed magnetic data curve (top panel) and gravity data curve (middle panel) along cross-sectional profile A-A' (bottom panel) from Taylor (2013). North is to the right. Abbreviations: QS=Quaternary sediments; CN=Chuckanut Formation; EA=Easton Metamorphic suite; BP=Bell Pass Mélange; CH=Chilliwack group; NK=Nooksack Formation; BBF=Birch Bay fault; DHF=Drayton Harbor fault.

Methodology

Gravity and Magnetic Data

Gravity data collected on the earth surface reflects density variations within the subsurface. Hence, gravity anomalies indicate rocks with different densities than the surrounding rocks. Gravity anomalies are useful in identifying subsurface structural features such as folds and faults. Magnetic data indicate rocks with different magnetic susceptibilities within the subsurface. For this reason, magnetic lineaments are indicative of faults or rocks with different magnetic susceptibilities juxtaposed to one another.

This study uses gravity data obtained from the U.S. Geological Survey (USGS) and other sources (e.g., Taylor, 2013). Aeromagnetic data used for the study were obtained from a database compiled by the USGS (R. Blakely, personal communication, 2015). The airborne magnetic data were collected in 1997 by a private company under USGS contract. The data were collected along north-south parallel lines spaced 400 m apart at an altitude of 250 m above the ground (Blakely et al., 1999). In addition, the study uses published geologic maps and cross-sections (Brown and Dragovich, 2003). These data provide information on subsurface rock types from which densities and magnetic susceptibilities can be estimated for modeling.

Data Processing

For this study, Geosoft's Oasis Montaj^{TM} with the GM-SYS modeling extension was used to process gravity and magnetic data by correcting, gridding, and mapping the compiled datasets. These grids were then used to create anomaly maps and cross-sectional profiles. The software provides dynamic linking, by which any location in map view can be viewed simultaneously on cross-sections.

All gravity data used in the study have been corrected using standard reduction procedures including terrain correction using digital elevation models (DEMs). Further details of these corrections can be found in Taylor (2013). Aeromagnetic data are expressed as total field anomaly (TFA) values. The magnetic datasets have been reduced to pole to correct for declination and inclination of the Earth's magnetic field in the area of the study. In this process, vertical component of the magnetic field is assumed to have a 90^0 inclination (Figure 10) to produce vertically polarized magnetic field (Bajgain, 2011).

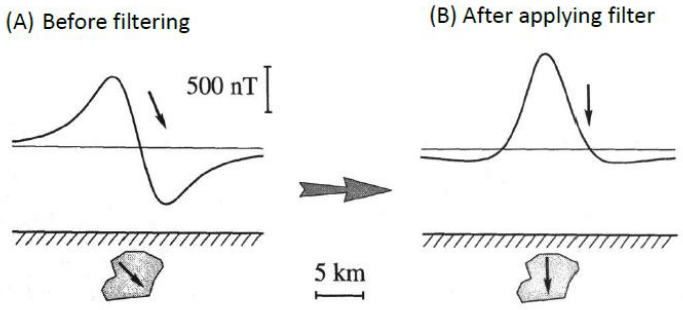

Figure 10. Illustration showing the effect of vertical component of magnetic field. A: Before correcting for reduced-to-pole and B: After correcting for reduced-to-pole (Bajgain, 2011; Blakely, 1995)

Wavelength-Separation Techniques

Different mapping techniques allow gridded data visualization and interpretation to be viewed more effectively. In this study, vertical derivative, upward continuation, and tilt derivative techniques have been used.

Derivative maps show the rate of change of potential fields along a certain direction. Hence, vertical derivative maps can indicate the rate of change of gravity or magnetic fields along the z direction. The order of differentiation enhances high wavenumber components of the spectrum (Oasis Montaj™: Magmap filtering, 2009). In this process, shallower subsurface structures associated with shorter wavelengths are more visible than the deeper structures with longer wavelengths. A low-pass filter is sometimes useful in removing noise. Vertical derivative maps help to identify shallow subsurface deformation, such as folds and faults, when combined with other filtering techniques such as upward continuation (Kinabo, 2007).

Like vertical derivative mapping, upward continuation is also useful for identifying shallow subsurface anomalous features and removing deeper, regional anomalies. It is applied by assuming that the gravity or magnetic fields are elevated to a certain height and subtracting that field from the original data. The remainder, or residual, captures shorter wavelength anomalies that reflect structures located nearer to the surface.

Tilt derivative is another wavelength separation technique that helps to locate the source and edge of magnetic anomalies from a reduced-to-pole magnetic field (Salem et al., 2010). The tilt angle of a magnetic anomaly, A, can be calculated as:

$$\theta = \tan^{-1}\frac{\frac{\partial y}{\partial z}}{\frac{\partial y}{\partial h}} \ldots\ldots\ldots\ldots\ldots\ldots\ldots\ldots\ldots\ldots\ldots\ldots \text{(1)}$$

Here the numerators and denominators are vertical and horizontal derivatives, respectively. The tilt angle, θ, is dependent on both the horizontal and vertical magnetization with equal weight; hence, both weaker and stronger magnetic anomalies are identified in this technique.

Data Modeling

Two transects, A-A' and B-B', from the gravity and magnetic regional datasets have been chosen parallel to the potential field gradients for cross-sectional modeling, thus avoiding three-dimensional effects (Figure 11a). Profile A-A' is oriented NE-SW and extends from the Canadian border on the north to the Lummi Island on the south. Profile B-B' is oriented N-S, with the northern end close to A-A'. The profile extends from the Canadian border on the north to Bellingham Bay in the south (Figure 11a). Along these profiles, both the observed gravity and magnetic data have been extracted for modeling. Because the gravity data consist of land-based measurements and are not evenly distributed, observed values along the cross-sectional profiles are interpolated between measured values.

Calculated gravity and magnetic curves are generated from polygons used to represent subsurface geologic bodies in the model. Density and magnetic susceptibility values are assigned to these polygons based on the inferred rock types or on empirically measured values (Telford et al., 1990, Kelsey et al., 2012). The rock types and geologic structure have been constrained by published geologic maps and cross-sections (Brown and Dragovich, 2003). The aim of the 2.5D modeling in this study is to achieve a best-fit between the observed data and calculated data curves based on the generated subsurface geologic bodies.

Results

Gravity Grid Maps

The Complete Bouguer Anomaly (CBA) map (Figure 11a) reflects a complex variation of densities in and around the Bellingham basin. Two broad northeast-southwest-trending gravity lows, namely anomaly (C, -97 mGal) and (D, -94 mGal), exist within the central part of the basin. These gravity lows indicate the deepest part of the Bellingham basin or low-density contrast of the rock unit than the surrounding rocks (Table 1). Anomaly (C) is separated from anomaly (D) to the east by a ridge of slightly higher values. The ridge is associated with a buried anticlinal structure within the Bellingham basin (Brown, and Dragovich, 2003). A prominent gravity high (E, ~ -44 mGal) occurs on the northern side of the area, along the border with Canada. Gravity appears to increase smoothly from the low areas (C and D) to the north (E). Two small anomalies (B) appearing on the western side of the basin appear to be offset by the Birch Bay fault (BB). A circular gravity high of about -60 mGal (G) exists on the southeastern side of the study area. Poor data coverage on the western part of the basin (white shaded area) and beyond the coastline limits interpretation in these areas. However, gravity values appear to increase significantly towards the southwest of the study area (anomaly (F), ~ -40 mGal) near the Lummi Island possibly due to a change in the rock composition: and the presence of an ophiolite complex.

The isostatic residual of the CBA map (Figure 11b) shows the deepest parts of the Bellingham basin and defines the overall basin's shape and extent. The gravity lows in the isostatic residual tends to follow an arcuate shape, extending towards the north at the eastern and western margins. It also shows two sub-basins or gravity lows within the deepest part and another sub-basin at the northeastern edge of the study area.

Magnetic Grid Maps

The TFA maps prepared from the gridded data are shown in Figures 12 and 13. Warmer colors indicate magnetic highs and cooler colors indicate magnetic lows. There are five major magnetic highs in the TFA map (Figure 12) which are mostly circular or sub-circular in shape. There are some magnetic lineaments indicating abrupt linear contrast of TFA value within the region. Most of these lineaments terminate against the magnetic highs. The lowest TFA values are seen in the southern (-460 nT) and eastern part (-330 nT) of the Bellingham basin area (Figure 13). One of the higher TFA values, anomaly (H, ~ 276 nT) lies towards the northern part of the area along the U.S.-Canada border. Another magnetic high, anomaly (I) (~145 nT), appears to be a continuation of anomaly (H), although it is separated by slightly lower values that are on strike with the projection of the Drayton Harbor fault. These circular magnetic highs are likely plutonic rocks with higher magnetic susceptibilities. based on their shape. A smaller, subcircular magnetic high (anomaly K, ~ 130 nT) occurs in the central part of the study area, but unlike the highs to the north, anomaly (K) is associated with a gravity low. This suggests that the rock units responsible for this high differ in composition from those in the north and possibly associated with pebble conglomerate rocks. A subcircular magnetic high (L) on the southeastern part with a value of 73.94 mGal provides evidence of buried ultramafic rocks (Kelsey et al., 2012). This study suggests the source of

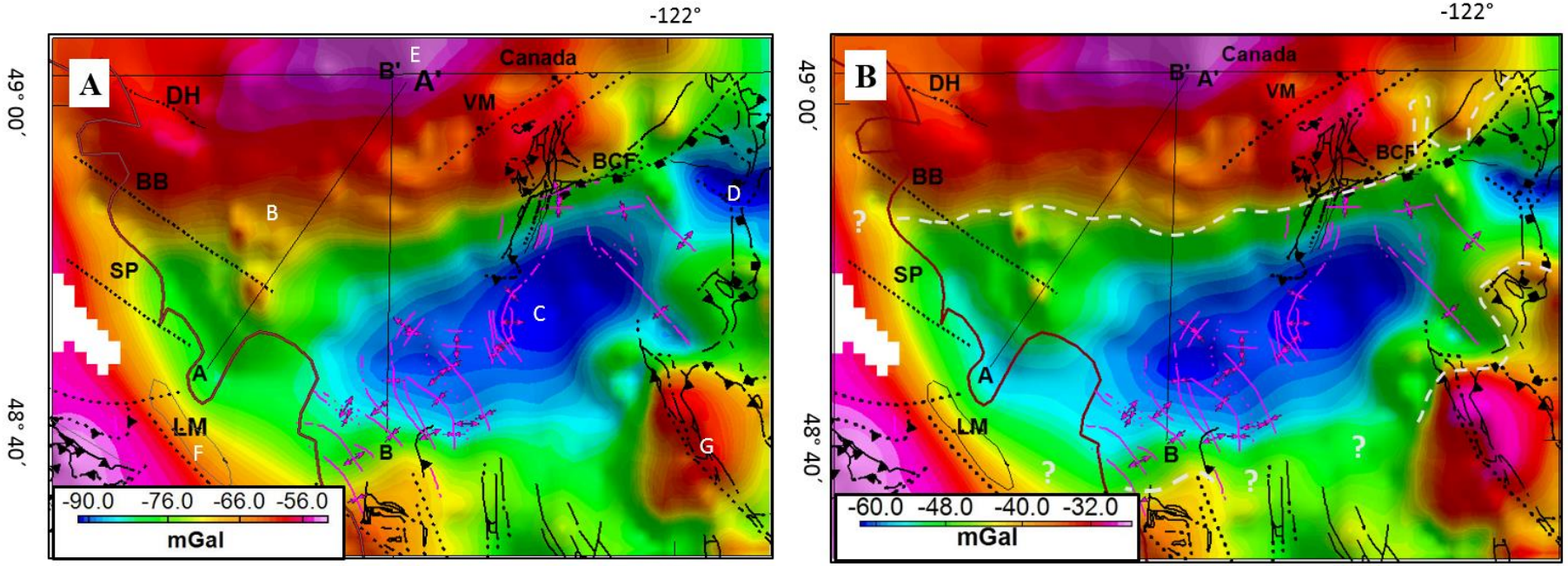

Figure 11. A: Complete Bouguer Anomaly (CBA) map of the study area. B: Isostatic Residual map of the Bellingham basin. Green lines=coastline. A-A', B-B'= profile locations. Black lines= faults (dotted where inferred) from Geology GIS Data and Databases | WA – DNR (https://www.dnr.wa.gov/programs-and-services/geology/publications-and-data/gis-data-and-databases; last accessed: July, 2019). Abbreviations: DH= Drayton Harbor fault; BB= Birch Bay fault; and SP= Sandy Point fault; VM= Vedder Mountain fault; BCF= Boulder Creek fault; LM= Lummi Island. Letters B, C, D, E and G refer to features discussed in text. White polygons= no data.

this anomaly is influenced by the presence of Twin Sisters Dunite close to the surface.

An unusually high magnetic anomaly (J) (~423 nT) is observed on the Lummi Island. Such values do not appear elsewhere in the study area, but are seen on islands to the southeast (anomaly M and N, ~585 nT; Figure 13). The islands include mostly ophiolite complexes, known as Fidalgo Complex (FC), consisting of peridotite, gabbro, quartz-diorite tonalite, radiolarian argillite, sedimentary breccia and some volcanic lithic sandstone (Brown and Dragovich, 2003) and can be accounted for such higher TFA values. Insufficient data create artifacts in some parts of the area, mostly at the international boundaries and offshore regions. A smelter operation at the western part of the area causes unusually high TFA values. Data surrounding this operation are masked.

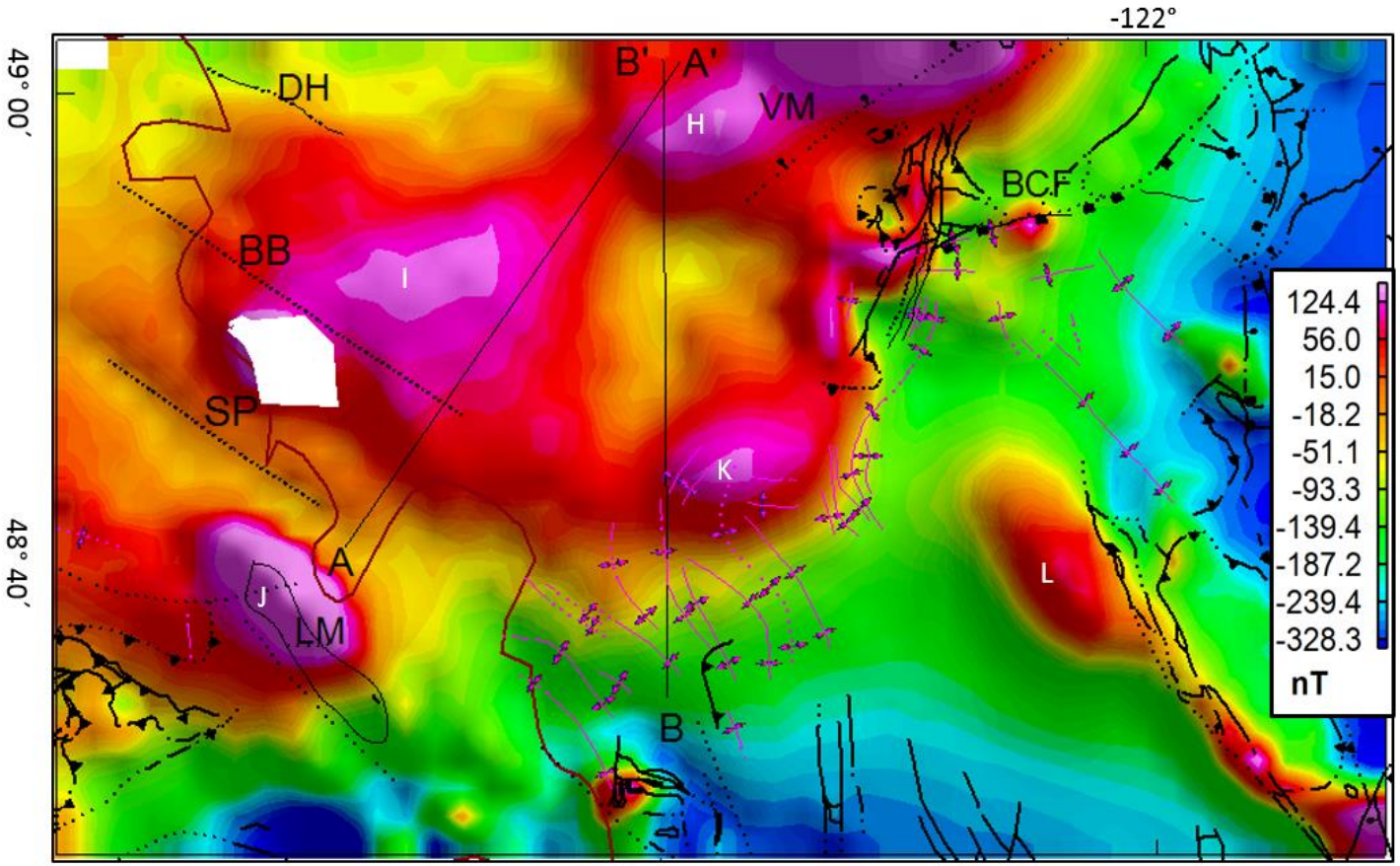

Figure 12. Total Field Anomaly (TFA) map of the Bellingham basin. H, I, J, K, and L are magnetic highs. Symbols and abbreviations as in Figure 11. Vertical white lines are artifacts due to cell size resolution. Anomaly H and I are associated with plutonic rocks with high magnetic susceptibility, possibly associated with the Bell Pass Mélange. J is associated with an ophiolite complex (Fidalgo Complex). Anomaly K may be is associated with pebble conglomerate rocks (Kelsey et al., 2012). Anomaly L is associated with buried ultramafic rocks (Twin Sisters Dunite).

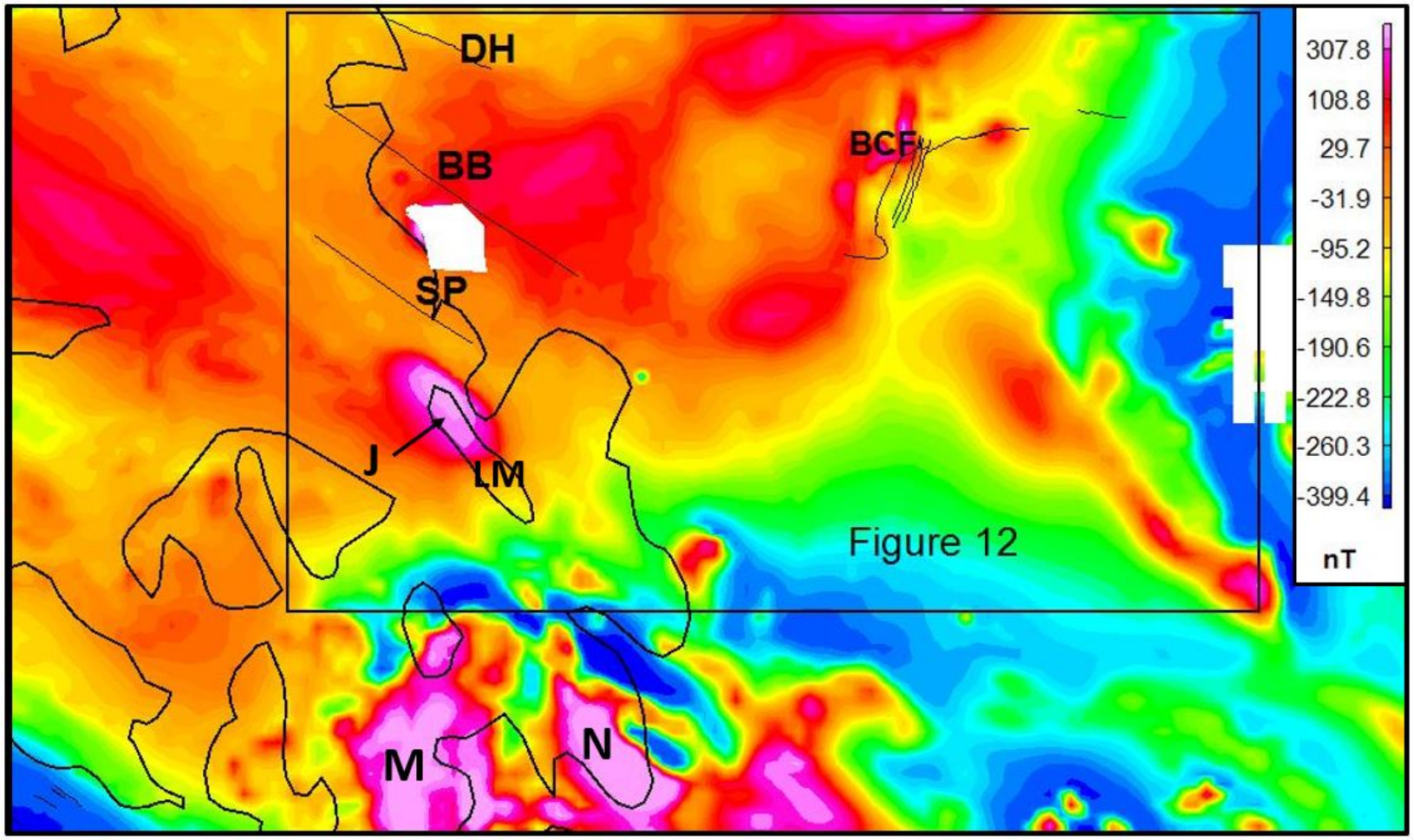

Figure 13. Total Field Anomaly (TFA) map of the Puget Sound region. Symbols and abbreviations as in Figure 11. J, M, N= magnetic highs caused by the exotic ophiolite complexes accreted to the upper plate. Vertical white lines are artifacts due to cell size resolution. Black square= extent of the study area in Figure 12. Vertical white lines are artifacts due to cell size resolution.

Wavelength-Filtered Maps

Vertical Derivative Map/ Upward Continued Map

The vertical derivative magnetic anomaly map (Figure 14) prepared for this study reveals several distinct lineations that might be associated with faults. Many of these lineations show a general northwest-southeast orientation (dotted lines in Figure 14a). One lineation intersects both profile A-A' and B-B' and is coincident with the location of the Drayton Harbor fault, as mapped by Kelsey et al. (2012). To the south, a second lineament corresponds to the mapped position of the Birch Bay fault in the study area. This lineation tends to disappear within a large area of magnetic highs but there is a subtle suggestion that it reappears on strike farther to the southeast. A pair of northwest-striking parallel lineaments occurs to the south of the Birch Bay fault. The first correlates with the mapped location of the Sandy Point fault. It strikes the profile line A-A' and extends well into the basin area. The second follows the same trend and separates a magnetic low on the north from a high on the south, forming a very high gradient in values. This lineation appears to correspond to a geologic contact with a mapped ophiolite complex (to the southwest) (dashed lines in Figure 14a). Several other lineations with similar orientations appear in the east side of the study area. These appear to form along thin, northwest-elongated features but do not correlate with mapped faults. Lastly, there is one southwest-northeast striking lineation in the northeast corner of the study area that lies along the mapped Vedder Mountain fault (VM).

The residual of the upward continued magnetic map (Figure 14b) also highlights magnetic anomalies that represent sources in the shallow crust. Here, the 100-m upward continued residual map shows similar lineaments as the vertical derivative map. However, the northern lineaments are more pronounced in the upward continued map than in the vertical derivative map. For example, the lineaments near the Vedder Mountain fault and the Boulder

Creek faults are more defined in the upward continued map. The extension of the Drayton Harbor fault to the eastern part of the area is also prominent in the residual map.

Tilt Derivative Map

A tilt derivative is applied to the TFA and the resulting map is shown in Figure 15. Although the tilt derivative anomaly map captures many of the same lineations and corresponding high gradients as the vertical derivative map, there are some distinct differences. Most of the lineaments are less continuous than in the vertical derivative map because rather than enhancing just the edges, tilt derivative mapping enhances both the edges and sources. In a few areas, the vertical derivative map shows a magnetic high, whereas the tilt derivative shows a magnetic low (e.g., northeastern section of the map). Similarly, the magnetic low in the northcentral part of the area in the tilt derivative map is shifted from its position in the vertical derivative map. Both techniques enhance the northwest-trending elongate magnetic high anomaly in the southeastern portion of the maps. This anomaly is associated with buried ultramafic rocks (Twin Sisters Dunite). Finally, although the gradient of values associated with the Sandy Point fault and the ophiolite complexes are prominent in all maps, it is more pronounced in the tilt derivative map.

Plotting zero contours on the tilt derivative map highlights the source bodies that correspond to the magnetic anomalies. Using this technique, a large part of the area that corresponds to the central basin has been identified as a major source of magnetic anomalies, due to the plutonic rocks (likely Easton Metamorphic Suite) in the Bellingham basin. In the southeastern part of the study area, Twin Sisters Dunite has been identified as another source. In the southwestern part, the ophiolite complexes in the offshore region have been identified

as another anomaly source. There are some other scattered anomaly sources on the eastern side that do not correspond to any known sources.

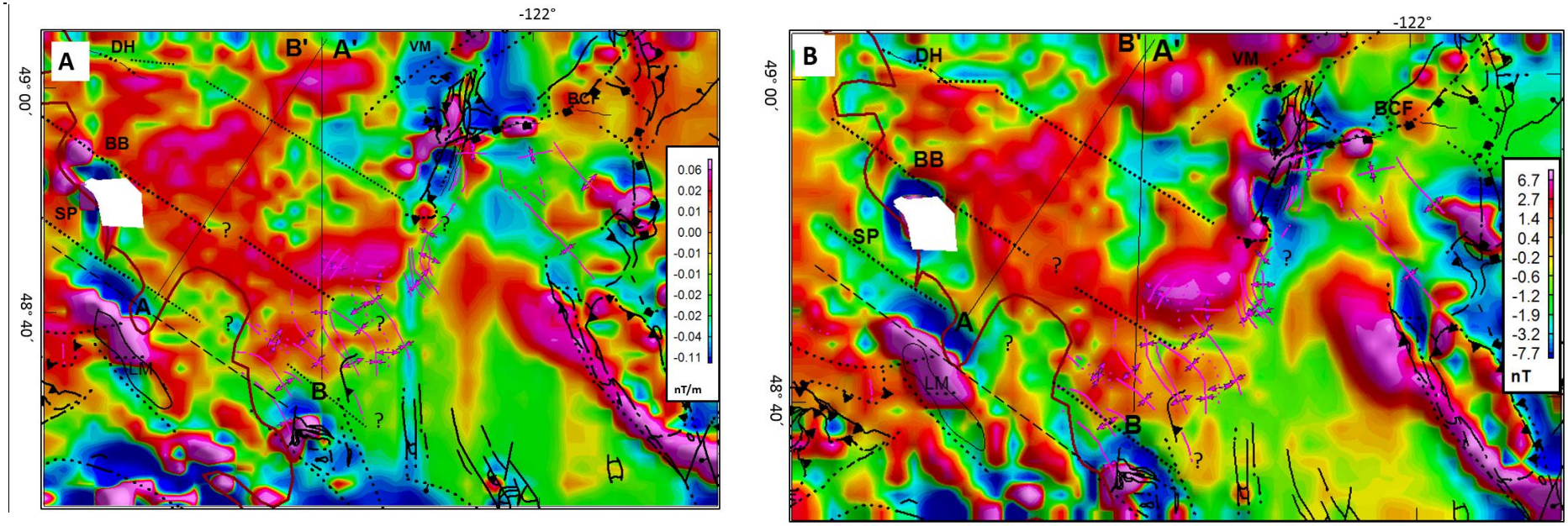

Figure 14. A: Map of TFA of the study area with vertical derivative filter applied. B: Residual map after upward continuing the TFA at 100 meters. Symbols and abbreviations as in Figure 11. Small dotted lines indicate inferred fault contacts. Note high gradients of values along mapped faults (e.g., DH, BB, SP, VM, and BCF).

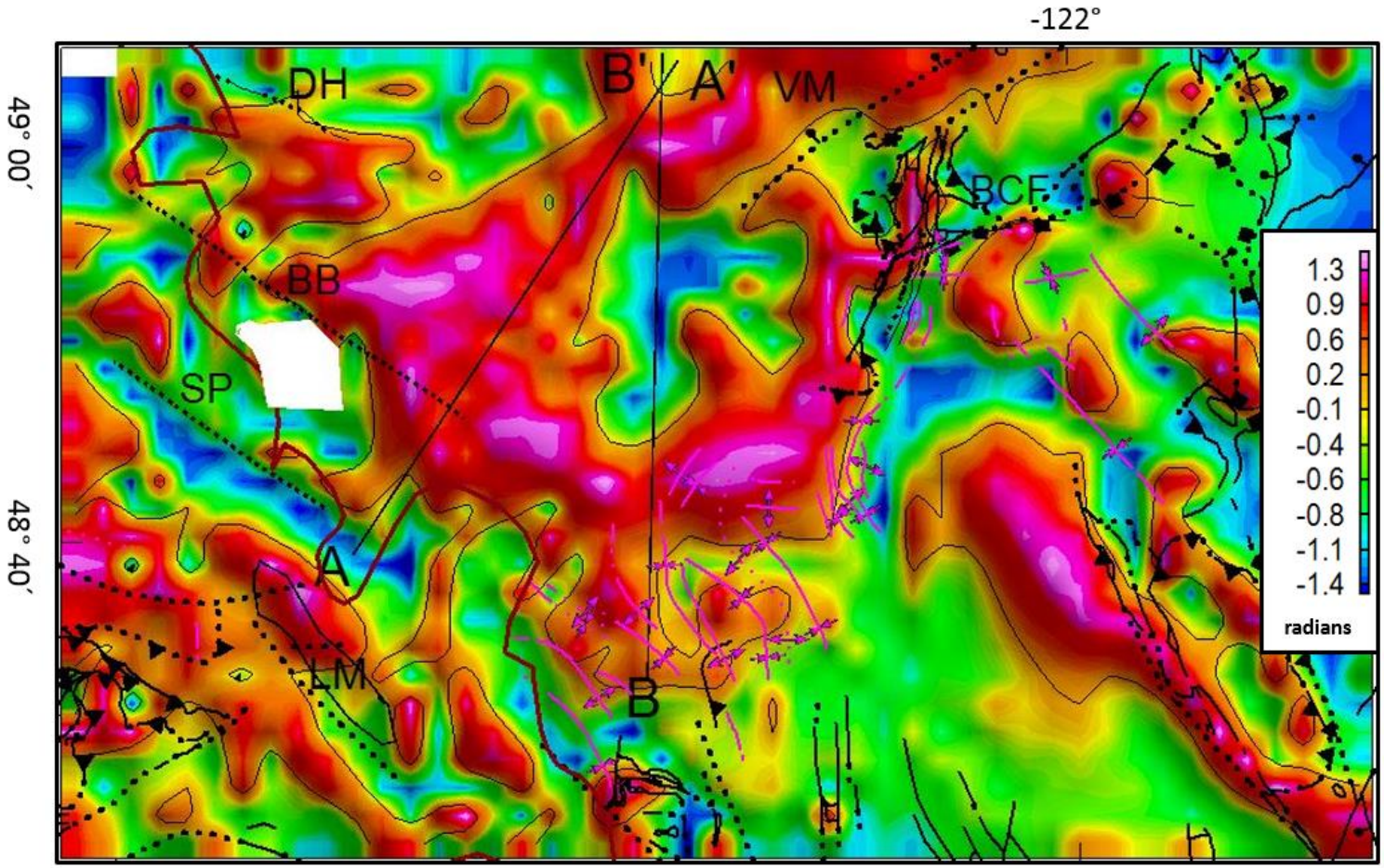

Figure 15. Tilt derivative map of the study area with zero contours, indicating source bodies of the magnetic anomalies. Symbols and abbreviations as in figure 11. Note large arcuate magnetic high in the central basin is attributed to buried plutonic rocks (Easton Metamorphic Suite). Linear magnetic highs in the southeastern of the study area is attributed to the buried ultramafic rocks (Twin Sisters Dunite). White Polygon= masked area over smelter operation. Vertical lines are artifacts due to cell-size selection.

Cross-Sectional Profiles

Cross-Sectional Profile A-A'

The northeast-southwest cross-sectional profile, A-A' (Figure 16), extends a distance of more than 35 km. The southern end of the profile is located close to the shoreline of the Bellingham bay and Lummi island. The northern end of this profile reaches close to the U.S.-Canada border and intersects the northern end of the profile B-B'. Along the profile, the TFA curve has an increasing trend from south to north. It reaches a value of 114 nT at about 16 km from A. The TFA value decreases to a low of 53 nT at about 25 km from the southern end of the profile or point A. A local maximum of 100 nT occurs at about 28 km from A, and then the curve decreases gradually towards the northern edge of the profile.

The observed gravity curve shows CBA values with an increasing trend from south (-78 mGal) to the north (-42 mGal), with very little variation. A slight high occurs at about 9 km from the profile's southern end, where the value increases to -68 mGal. The trend then continues to increase gradually towards the northern part of the profile.

Six geometric bodies have been created to represent rock units, with densities and magnetic susceptibilities appropriate for their compositions and rock types. The rock descriptions and relative layer thicknesses have been obtained from Brown and Dragovich (2003), and respective densities (Telford et al., 1990) along with empirically measured magnetic susceptibility values (Kelsey et al., 2012) were provided (Table 2). Previous models suggest all models extend throughout the basin along the profile (Brown and Dragovich, 2003). All the rock units are more or less deformed along the profile with two major anticlinal folds occurring at a distance of 1.2 km and 8.6 km from the southern end. These folds correspond to anomalies associated with the Sandy Point and the Birch Bay faults,

respectively. The projected location of the on-strike intersection of the Drayton Harbor fault with the cross-section shows little to no deformation. A local maximum in the magnetic anomaly curve corresponds to a third anticlinal fold in the cross–section at ~ 28 km along the profile. This fold corresponds to a pronounced high in the vertical derivative map (Figure 14a).

Cross-Sectional Profile B-B'

Cross-sectional profile B-B' (Figure 17) extends for a length of about 34 km. The profile is oriented north-south and the northern end intersects with the profile A-A'. From southern end towards north, both the gravity and magnetic observed curves show variations of CBA and TFA values and have an increasing trend from the south to north. Along the cross-sectional profile, there is a gradual increase of magnetic values, reaching a peak of about 68 nT at 10 km from the southern end of the profile. The value then decreases until it reaches a value of about -50 nT at about 22 km from the southern end. The curve then gradually increases again until it reaches a maximum value at value of about 136 nT at 29 km along the profile. The lowest value along the profile is -99.85 nT. The observed gravity curve starts with a decreasing trend from the southern end of the profile and reaches a value of -88 mGal at a distance of about 8 km. Then the curve gradually increases until it reaches a maximum value at of -47m mGal at the profile's northern end.

The subsurface rock units have been created with the same rock description as in profile A-A', as described in Table 2 (Brown and Dragovich, 2003). The cross-sectional profile B-B' indicates two major anticlinal folds for the units at a distance of about 10 km and 30 km from the southern end of the profile. A third anticline is observed at about 5 km from the southern end or point B. The fold at 5 km from B tends to be influenced by the Sandy

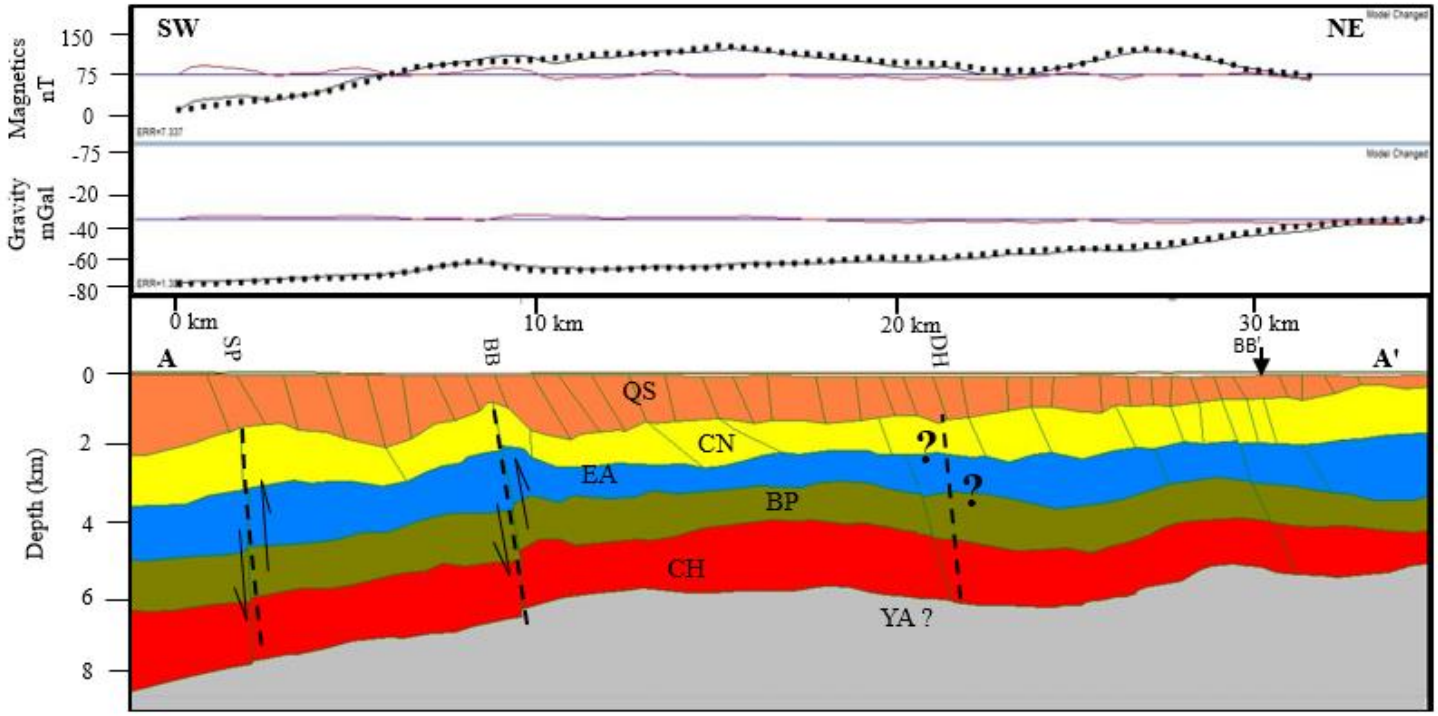

Figure 16. Top: Total field anomaly (TFA) data along profile A-A' showing observed (dots) and calculated values (line). Middle: Complete Bouguer anomaly (CBA) gravity data along profile A-A' showing observed (dots) and calculated values (line). Bottom: geologic interpretation of best-fit model (VE=0.8). Dashed black lines= interpreted faults. Arrows indicate relative movements along faults. Abbreviations: QS= Quaternary sediments; CN= Chuckanut Formation; EA= Easton Metamorphic Suite; BP= Bell Pass Mélange; CH=Chilliwack Group; YA= Yellow Aster Complex; SP= Sandy Point fault; BB=Birch Bay fault; DH= Drayton Harbor fault. Dark black downward arrow indicates point of intersection with the profile BB'.

Point fault but has been modeled as a reverse fault with the northern side up. The fold at 10 km from the southern end corresponds to the Birch Bay fault and has been modeled as the northern side up. The location where the Drayton Harbor fault intersects the profile, does not indicate significant deformation in terms of offsets or folding. Hence, it has been modeled as a vertical fault with strike slip movement.

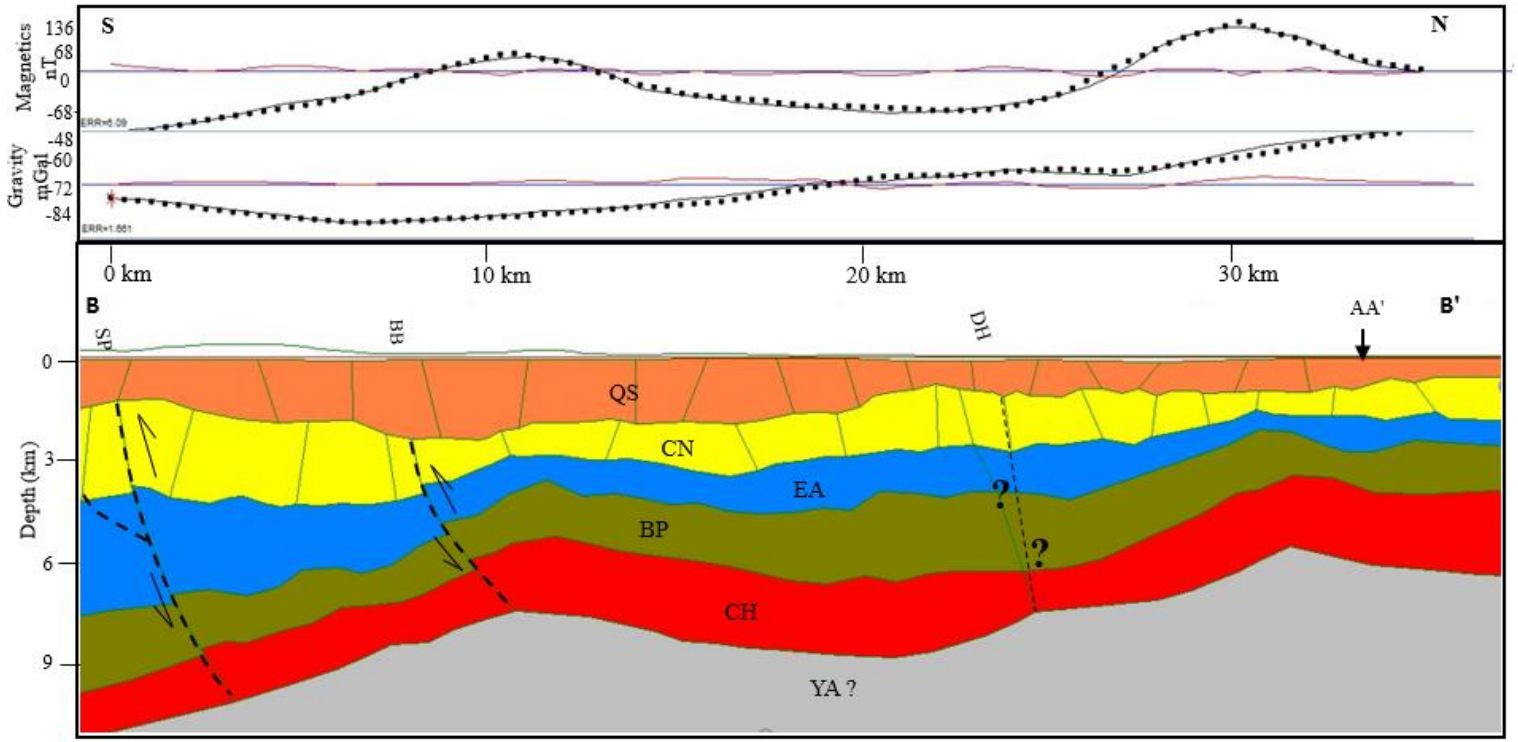

Figure 17. Top: Total Field Anomaly (TFA) data along profile B-B' showing observed (dots) and calculated values (line). Middle: Complete Bouguer Anomaly (CBA) gravity data along profile B-B' showing observed (dots) and calculated values (line). Bottom: geologic interpretation of best-fit model (VE=0.9). Dashed black lines=faults. Arrows indicate relative movements along faults. All the symbols and abbreviations as in figure 16. Dark black downward arrow indicates point of intersection with the profile AA'.

Table 2. Modeled rock units for the cross-sectional profiles A-A' and B-B' with their lithologies, densities, and magnetic susceptibilities.

Geological Units	Time	Rock Types	Densities (kg/m^3)	Magnetic Susceptibilities (SI)	Maximum Thickness (km)
Glacial and Alluvial Sediments	Quaternary	Previously deposited units of all Types (Igneous, Sedimentary, and Metamorphic)	2000	0.001-0.007	1.5-3
Chuckanut Formation	Tertiary	Arkosic Sandstone, Siltstone, Conglomerate, and Coal (Mostly Fluvial)	2500	0.00001-0.005	1.2-3
Easton Metamorphic Suite	Jurassic	Metabasalts, Metatuffs, Metagraywacke, Siliceous Carbonaceous Phyllites	2800	0.0003-0.001	2.2-5
Bell Pass Mélange/ Orcas Chert	Triassic-Middle Jurassic	Mudstone, Pillow Basalts, Limestones, Volcanic Lithic Clastic Rocks	2700	0.04-0.05	0.5-2.5
Chilliwack Group/East Sound Group	Devonian-Permian	Volcanic Rocks with Sandstones, Siltstones, Limestones	2800	0.09	2-2.8
Yellow Aster Complex	Pre Devonian to Devonian	Siliceous garnet-pyroxene gneiss, calc-silicates, marble, gabbro-tonalite plutonic rocks, and basalt andesites.	2670	0.01	------

Discussion

The results of this study provide insight into the geometry and deformational history of the Bellingham basin and support the hypothesis that Holocene-active faults (Kelsey et al., 2012) observed along the coastline of northwestern Washington extend well into the basin proper. Structural features described in previous work and analysed in this study are described below.

Geometry of the Bellingham Basin

Early work included the Bellingham basin within the much larger Georgia basin (Gallup, 1957; Kelsey et al., 2012). Although this study places the eastern boundary of the Bellingham basin in the same location as previous work (Figure 2 in Kelsey et al., 2012), the results of the isostatic residual gravity field (Figure 11b) suggest that the northern boundary of the Bellingham basin is farther to the south than previously proposed by Gallup (1957) and shown in Kelsey et al. (2012). Both Gallup (1957) and Kelsey et al. (2012) defined the northern boundary of the Georgia basin as positioned between Vancouver and the Coast Ranges of British Columbia. In this study, the Bellingham basin appears as a relatively small, arcuate-shaped basin, similar in size to other forearc basins to the south. This geometry is consistent with a model proposed by Taylor (2013), suggesting that the Bellingham basin is at best only a part of the larger structure. Two major gravity lows (anomalies C and D in Figure 11) define the deepest parts of this basin. Although the eastern, northern and southern

boundaries appear well-defined, a lack of offshore gravity data makes the location of the western boundary unconstrained by this study.

Early work also asserted that the Devil's Mountain fault to the south marked the boundary between north-directed compression against a stable "buttress" (Johnson et al., 2001). However, later work by Barnett et al. (2006) on the Boulder Creek fault within the Bellingham basin, along with more recent results from GPS campaigns (e.g., McCaffrey et al., 2013) suggest that the stable buttress must be located farther to the north.

Cross-sectional modeling performed in this study suggests that anticlinal folding has affected Cretaceous and younger strata within the basin. Although not unique, results of the potential field modeling are consistent with the hypothesis that folding and faulting is continuing in order to accommodate ongoing strain (McCaffery et al., 2013; Kelsey et al., 2012). Polivka (2015) in his analysis of offshore seismic reflection data interpreted offsets in shallow reflectors as growth faults, which he interpreted as proof of ongoing deformation. Based on potential field data used in this study, however, the cross-sectional models proposed here do not have the resolution to support or refute this hypothesis.

Active Faults within the Bellingham basin

The vertical derivative, residual upward continued map and tilt derivative maps produced in this study identify pronounced lineaments that can be associated with the five major faults mapped within the Bellingham basin. Each of these is discussed below.

Boulder Creek fault (BCF)

On the northeast part of the basin, the Boulder Creek fault system is positioned near the interpreted northern boundary of the Bellingham basin. A pronounced gradient is seen in the vertical derivative map of magnetic data along the mapped fault trace (Figure 14a).

Kelsey et al. (2012) notes that although long-term displacement on the BCF is northside up, the work of Barnett et al. (2006) suggests that the most recent displacement along the fault is southside up, which is inconsistent for a fault bounding the basin on its north side. The results of this study support the BCF as the northeastern boundary of the Bellingham basin and note that a change in relative motion along the fault may be the result of recent motion related to oblique subduction and clockwise rotation within the upper crust created by oblique plate interactions. More paleoseismologic and geomorphic studies of the BCF are needed to understand better the role of the BCF in the basin's evolution.

Vedder Mountain fault (VM)

The Vedder Mountain fault was identified by Dragovich et al. (2002), an inferred contact in between the Vedder Mountain and the Quaternary sediments (QS), as a steeply (>45º) dipping normal fault, with the northwest side down. There is a northeast-southwest trending magnetic lineament identified by Kelsey et al. (2012) along that fault. Although all wavelength filtering techniques show this lineament, the residual of the upward continued magnetic field map (Figure 14b) indicates a prominent lineament along this fault.

Drayton Harbor fault (DH)

The Drayton Harbor fault has been identified from the prominent lineaments in magnetic data and LiDAR data (Kelsey et al., 2012). Lineaments seen in the TFA and vertical derivative maps produced in this study suggest that the Drayton Harbor fault continues along a southeast trajectory for at least 30 km, in agreement with previous estimates (Kelsey et al., 2012). At this distance, the lineament appears to lose definition at an area of magnetic highs. Little is known about the deformation pattern of the Drayton Harbor fault since its recent discovery by Kelsey et al. (2012). Using newly acquired LiDAR data, Kelsey et al. (2012) inferred northside-down vertical displacement.

Cross-sectional profiles A-A' and B-B' modeled in this study do not require any significant deformation at the location where the projected magnetic lineament associated with the Drayton Harbor fault crosses the profiles. Lack of vertical deformation can be explained, however, by assuming strike-slip motion along the Drayton Harbor fault. Interestingly, the projected strike of the Drayton Harbor lineament is matched by a magnetic contact associated with the Twin Sisters range, although there is no evidence provided in this study to support a relationship. An alternative interpretation is that the Drayton Harbor lineament curves to the northeast as it enters the basin from the west and connects with high gradients, perhaps by transform structures observed near Sumas, to the north of the postulated basin's northern boundary. These options cannot be explored further, however, given the limitations of the available data.

Birch Bay Fault (BB)

In this study, the Birch Bay fault appears as a magnetic lineament on the vertical derivative map (Figure 14a). The northern side of the fault is associated with the Birch Bay anticline (Figure 3; Hurst, 1991). Based on paleoseismic data, LiDAR imaging, and aeromagnetic anomaly mapping, Kelsey et al. (2012) the estimated length of the Birch Bay fault as about 24 km. However, this study suggests that the Birch Bay fault is greater than 45 km long, if the length includes its offshore extension as interpreted by Polivka (2013). The cross-sectional models along profiles A-A' and B-B' show the Birch Bay fault as a north-dipping, low-angle reverse fault. This interpretation is consistent with one interpreted from a nearby published seismic line (Hurst, 1991). This observation is also consistent with compression and rotation dextral motion of western Washington from GPS measurement (McCaffrey et al., 2013). However, this study does not provide support for the interpretation that the Birch Bay fault is a growth fault with a strike-slip component (Polivka, 2013).

Sandy Point fault (SP)

The Sandy Point fault, first identified by Kelsey et al. (2012), appears as a prominent magnetic lineament on both the vertical derivative and tilt derivative magnetic maps. The lineament on such wavelength filtered maps identified this fault as a shallow subsurface fault buried under the younger sediments (QS). The magnetic lineament associated with the fault extends into the basin for more than 24 km based on these maps. Combining the offshore seismic lines (Polivka, 2015), the fault length can be measured as more than 45 km. Kelsey et al. (2012) interpreted three coseismic displacements based on uplifted Holocene shorelines observed along a coastal transect. North of the fault is the Sandy Point anticline, which is thought to be of Quaternary age (Kelsey et al., 2012). Although cross-sectional profile B-B' does not show the projection, profile A-A' shows the Sandy Point fault as a low-angle, north-dipping reverse fault (Figure 16). The development of the Sandy Point anticline is possibly the result of subsurface deformation by this reverse faulting.

Based on his analysis of two marine seismic reflection lines, Polivka (2013) interpreted the Sandy Point fault as a reverse fault associated with the San Juan thrust system. This interpretation also showed the Sandy Point and Birch Bay faults originating from a crustal detachment (Fig. 7b, Polivka, 2013). Based on these seismic lines and the presence of a magnetic lineament extending to the west, the Sandy Point fault is assumed to extend well beyond the coastline; however, this study provides no evidence to support a major crustal detachment.

Marine seismic line W2 (Figure 7b) interpreted by Polivka (2013) also showed loss of reflector coherency on the southern part of the Sandy point fault. Polivka (2013) explained this as steeply dipping beds near Lummi Island causing a magnetic high. However, this study suggests the ophiolite complexes near the Lummi Island cause such high anomalies and seen as a distinct lineament on the wavelength filtered maps (dashed lines in Figure 14).

Table 3. Fault lengths within and outside of the Bellingham basin by Kelsey et al. (2012) compared to the results of this study.

Fault names	Length identified by Kelsey et al. (2012) (km)	Length identified in this study (km)	Length identified by combining offshore seismic lines (km)
Drayton Harbor	25	~30+	Not mapped
Birch Bay	24	~30+	~45+
Sandy Point	12	24+	~45+

Implications for earthquake hazard

The results from this study support the work of Kelsey et al. (2012), who proposed the existence of three new faults, Drayton Harbor, Birch Bay, and Sandy Point, in the Bellingham basin. Although Holocene movement on these faults has been documented by their previous studies along the coast, the dimensions of the faults are based mainly on magnetic data and the assumption that magnetic lineaments, or magnetic "contacts," can represent faults by juxtaposing different rock types. It should be noted, however, that not all lineaments are faults. Thus, confirmation by field mapping is essential for distinguishing among sources for the lineations seen in the data.

Field studies by Kelsey et al. (2012) suggest that the Birch Bay and Sandy Point faults were active at least 1200 yr. B.P. based on evidence of vertical displacement. Although earthquakes along these faults have not exceeded M=3 since instrumental recording began in 1969, there is evidence of lower magnitude seismicity along the Birch Bay and Sandy Point faults as well as scattered seismicity throughout the deep basin (Figure 2). In the year 1990, an M =5.0 earthquake occurred near the eastern margin of the Sumas Mountain, near the

town of Deming, Washington, and ~ 7 km southeast of the Boulder Creek fault (Figure 2). The focal mechanism of this earthquake was as oblique-reverse slip along a northeast trending fault (PNSN Events | Pacific Northwest Seismic Network (https://pnsn.org/events?custom_search=true; last accessed: July, 2019)). A large cluster of aftershocks lasted for more than ten days (Figure 2). How or if the Deming swarm is related to the Boulder Creek fault is not apparent. If the Boulder Creek fault represents the Bellingham basin boundary, the Deming event and related earthquakes could represent deformation in the form of crustal block extrusion resulting from present-day compression and rotation (Sherrod et al., 2013).

Earthquake relocation in northwestern Washington might provide useful information about the relationship of observed seismicity with the Birch Bay and Sandy Point faults. Deformation identified from the cross-sectional models developed in this study support the sense of motion described in Kelsey et al. (2012) and suggest that the Birch Bay and Sandy Point faults continue for at least 30 km and 24 km, respectively into the basin. Using the empirical relationships of Wells and Coppersmith (1994) and results of his field study, Kelsey et al. (2012) suggested that the Birch Bay fault produced an earthquake with magnitude of 6.0-6.5 in the past. Because this study estimates a greater length for the Birch Bay fault, it may be capable of generating a higher magnitude earthquake. In addition, if the interpretation of the length of the Sandy Point is accurate, it too may be capable of producing a moderate to large magnitude earthquake.

Conclusion

Based on the isostatic residual calculated from the complete Bouguer gravity data, the shape and extent of the Bellingham basin can be described as an arcuate-shaped, east-west-trending basin positioned between the Canada and Washington. Limited availability of offshore data, however, precludes knowledge of the basin's configuration to the west. Results of the study suggest that the Boulder Creek fault functions as the northern basin boundary in the eastern section of the study area.

Magnetic anomalies indicate that the basin is composed of several rock units juxtaposed to one another to create magnetic lineations or "contacts" that are observable in the data subjected to wavelength filtering. Some of these lineaments are coincident with mapped faults that extend into the basin. The existence of three major faults, Drayton Harbor, Birch Bay and Sandy Point, recently discovered from LiDAR imagery and field studies (e.g., Kelsey et al., 2012) are supported by the results of this study. Two cross-sectional models resulting from this analysis suggest both the Sandy Point and the Birch Bay faults can be modeled as reverse faults with north-side up offsets, as seen in previous work along the western Washington coast (Kelsey et al., 2012). However, there is no justification for vertical offset in the model at the projected intersection of the Drayton Harbor fault and the cross-section. This implies that either the Drayton Harbor fault does not extend far into the deep basin, or alternatively, the fault motion is predominantly strike-slip.

Epicentral locations of earthquakes within the Bellingham basin show a cluster of events around the Boulder Creek fault in the eastern part of the study area. Most of these earthquakes are related to the 1990 M = 5 Deming earthquake, which occurred about 7 km from the Boulder Creek fault. Although most other seismicity in the basin is scattered and of low magnitude, several epicenters appear to align along the Birch Bay fault. The last identified earthquake along the Birch Bay fault was a magnitude 6.0 at 1280-1070 yr. B.P. (Kelsey et al., 2012). Together, these observations suggest that the Birch Bay fault is currently active.

Although some epicenters are located near the trace of the Sandy Point fault, their relationship to the fault is not obvious. However, if the length of the fault (as estimated by the length of the magnetic lineament) is combined with its mapped location offshore (Polivka, 2013), then the Sandy Point fault could be capable of a much larger earthquake.

This study can be further improved by extending the cross-sectional profiles to the south beyond the inferred trace of the Sandy Point fault. In addition, analyses of offshore potential field and seismic data would aid in estimating the length of the three recently discovered faults in the Bellingham basin. Adding data from Canada and offshore islands would help to constrain the existing fault structures as well as the geometry of the basin to the west. Finally, relocating earthquakes in the basin using advanced methods for handling low-magnitude earthquakes would aid in determining the relationship of seismicity with existing faults.

References

Atwater, B.F., Tuttle, M.P., Schweig, E.S., Rubin, C.M., Yamaguchi, D.K., Hemphill-Haley, E., 2003, Earthquake recurrence inferred from paleoseismology: Developments in Quaternary Sciences, v. 1, p. 331-332.

Barnett, E.A., Kelsey, H.M., Sherrod, B.L., Blakely, R.J., Hughes, J.F., Schermer, E.R., Haugerud, R.A., Weaver, C.S., and Siedlecki, E., 2006, Active faulting at the northeast margin of the greater Puget lowland: A paleoseismic and magnetic-anomaly study of the Kendall scarp, Whatcom County, Northwest Washington: Eos Transactions AGU, Fall Meeting Supplements, Abstract S31A-0183,87(52).

Bajgain, S.K., 2011, Gravity and magnetic modeling of basement beneath Alabama Gulf Coastal Plain [MS thesis]: Auburn University, 88 p.

Blakely, R.J., 1995, Potential theory in gravity and magnetic applications: New York, Cambridge University Press, 437 p.

Blakely, R.J., Wells, R.E., and Weaver, C.S., 1999, Puget Sound aeromagnetic maps and data: U.S. Geological Survey Open File Report, 514 p.

Blakely, R.J., Wells, R.E., Weaver, C.S., and Johnson, S.Y., 2002, Location, structure, and seismicity of the Seattle fault zone, Washington: Evidence from aeromagnetic anomalies, geologic mapping, and seismic reflection data, Geological Society of America Bulletin, v. 114, p. 169–177.

Blackwell, D.L., 1983, Geology of the Park Butte–Loomis Mountain area, Washington (eastern margin of the Twin Sisters Dunite): [MS thesis]: Western Washington University, p. 253 p.

Booth, D. B., 1994, Glaciofluvial infilling and scour of the Puget lowland, Washington, during ice-sheet glaciation: Geology, v. 22, p. 695–698.

Brocher, T.M., Blakely, R.J., and Wells, R.E., 2004, Reinterpretation of the Seattle uplift, Washington, as a passive roof duplex: Bulletin of the Seismological Society of America, v. 94, p. 1379–1401.

Brown, E. H., 1986, Geology of the Shuksan suite, North Cascades, Washington, U.S.A. *in* Evans, B.W, Brown, E. H., eds., Blueschists and eclogites: Geological Society of America Memoir, v. 164, p. 143-154.

Brown, E.H., 1987, Structural geology and accretionary history of the Northwest Cascades system, Washington and British Columbia: Geological Society of America Bulletin, v. 99, no. 2, p. 201- 214.

Brown, E.H., and Dragovich, J.D., 2003, Tectonic elements and evolution of northwest Washington: Washington Division of Geology and Earth Resources, Geologic map GM-52.

Bucknam, R.C., Hemphill-Haley, E., and Leopold, E.B., 1992, Abrupt uplift within the past 1,700 years at southern Puget Sound, Washington: Science, v. 258, p. 1611–1614.

DeMets, D., Gorden, R.G., Argus, D.F., and Stein, S., 1994, Effect of recent revisions to the geomagnetic reversal time scale on estimates of current plate motions: Geophysical Research Letters, v. 21, p. 2191–2194.

Dragovich, J.D., Logan, R.L., Schasse, H.W., Walsh, T.J., Lingley Jr., W.S., Norman, D.K., Gerstel, W.J., Lapen, T.J., Schuster, J.E., and Meyers, K.D., 2002, Geologic map of Washington, Northwest quadrant: Washington Division of Geology and Earth Resources, Olympia, Geological Map GM-50.

Easterbrook, D.J., 1976, Geologic map of western Whatcom County, Washington: U.S. Geological Survey Miscellaneous Investigations Map, I-854-B, scale 1:62,500.

Finn, C., 1990, Geophysical Constraints on Washington Convergent Margin Structure: Journal of Geophysical Research, v. 95, no. B12, p. 19533-19546.

Gallup, W.B. (1957), Will these sedimentary basins [Pacific Coast] prove oil bearing?: The Oil and Gas Journal, v. 55, p. 142.

Gresens, R.L., Naeser, C.W.; Whetten, J.T., 1981, Stratigraphy and age of the Chumstick and Wenatchee Formations—Tertiary fluvial and lacustrine rocks, Chiwaukum graben, Washington: Geological Society of America Bulletin, v. 92, no. 5, part II, p. 841-876.

Haugerud, R.A., Sherrod, B.L., Wells, R.E., and Hyatt, T., 2005, Holocene displacement on the Boulder Creek fault near Bellingham, Washington and implications for kinematics of deformation of the Cascadia forearc: Geological Society of America Abstract Programs, v. 37(7), p. 476.

Haugerud, R.A., Harding, D.J., Johnson, S.Y., Harless, J.L., and Weaver, C.S., 2013, High resolution LiDAR topography of the Puget Lowland, Washington – A bonanza for earth science: GSA Today, v. 13, no. 6, p. 4-10.

Hurst, P.D., 1991, Petroleum geology of the Bellingham basin, Washington, and evaluation of the AHEL and Partners Birch Bay No. 1 well: Washington Geology, v. 19, p. 16–18.

Ichinose, G.A., Thio, H.K., and Somerville, P.G., 2004, Rupture process and near-source shaking of the 1965 Seattle-Tacoma and 2001 Nisqually, intraslab earthquakes: Geophysical Research Letters, v. 31, L10604.

Johnson, S.Y., Potter, C.J., Armentrout, J.M., Miller, J.J., Finn, C.A., and Weaver C.S., 1996, The southern Whidbey Island Fault: An active structure in the Puget lowland, Washington: Geological Society of America Bulletin, v. 108, p. 334–354.

Johnson, S.Y., Dadisman, S.V., Mosher, D.C., Blakely, R.J., and Childs, J.R., 2001, Active tectonics of the Devils Mountain fault and related structures, northern Puget lowland and eastern Strait of Juan de Fuca region, Pacific Northwest: U.S. Geological Survey Professional Papers, v. 1643, p.45.

Johnson, S.Y., Nelson, A.R., Personius, S.F., Wells, R.E., Kelsey, H.M., Sherrod, B.L., Koehler R., Witter R.C., Bradley, L.A., and Harding, D.A., 2004, Evidence for late Holocene earthquakes on the Utsalady Point Fault, northern Puget lowland, Washington: Bulletin of Seismological Society of America, v. 94(6), p. 2299–2316.

Kelsey, H.M., Sherrod B.L., Johnson S.Y., and Dadisman S.V., 2004, Land-level changes from a late Holocene earthquake in the northern Puget lowland, Washington: Geology, v. 32, p. 469–472.

Kelsey, H.M., Sherrod, B.L., Blakely R.J., and Haugerud, R.A., 2012, Holocene faulting in the Bellingham forearc basin: Upper plate deformation at the north of Cascadia subduction zone: Journal of Geophysical Research, v.117, B3049.

Kinabo, B.D., 2007, Incipient continental rifting: insights from the Okavango Rift Zone [Ph.D. dissertation]: Rolla, University of Missouri, 68 p.

Mazzotti, S., Dragert, H., Hyndman, R., Miller, M.M., and Henton, J., 2002, GPS deformation in a region of high crustal seismicity: N. Cascadia forearc: Earth Planetary Science Letters., v. 198, p. 41–48.

McCaffrey, R., King, R.W., Payne, S.J., and Lancaster, M., 2013, Active tectonics of northwestern U.S. inferred from GPS-derived surface velocities: Journal of Geophysical Research, v. 118, p. 709–723.

Misch, P., 1966, Tectonic evolution of the northern Cascades of Washington—A west-cordilleran case history, *in* Canadian Institute of Mining and Metallurgy: A symposium on the tectonic history and mineral deposits of the western Cordillera in British Columbia and neighbouring parts of the United States, Vancouver, 1964: Canadian Institute of Mining and Metallurgy Special Volume 8, p. 101-148, 1 plate.

Nelson, A.R., Johnson S.Y., Kelsey H.M., Wells R.E., Sherrod B.L., Pezzopane S.K., Bradley L., Koehler R.D., and Bucknam R.C., 2003, Late Holocene earthquakes on the Toe Jam Hill fault, Seattle fault zone, Bainbridge Island, Washington: Geological Society of America Bulletin, v. 115, p. 1388–1403.

Oasis Montaj, 2009, Magmap filtering: https://www.geosoft.com/media/uploads/resources/brochures/OM_MMF_fs_2009_10_web.pdf (last accessed July, 2019).

Polika, P., 2013, Tectonics of the Georgia Basin, northwest Washington State, USA, and southwest British Columbia, Canada [MS thesis]: University of Washington, 64 p.

Pratt, T.L., Johnson, S., Potter, C., Stephenson, W., and Finn, C., 1997, Seismic reflection images beneath Puget Sound, western Washington State: The Puget lowland thrust sheet hypothesis: Journal of Geophysical Research, v. 102, no. B12, p. 27,469–27,489.

Salem, A., Williams, S., Samson, Esuene, Fairhead, D., Ravat, D., and Blakely, R.J., 2010, Sedimentary basins reconnaissance using the magnetic tilt-depth method: Exploration Geophysics, v. 41, p. 198-209.

Satake, K., Shimazaki, K., Tsuji, Y., and Ueda, K., 1996, Time and size of a giant earthquake in Cascadia inferred from Japanese tsunami records of January 1700: Nature, v. 379, p. 246–249.

Sherrod, B. L., Bucknam R. C., and Leopold E. B., 2000, Holocene relative sea-level changes along the Seattle Fault at Restoration Point, Washington: Quaternary Resources, v.54, p. 384–393.

Sherrod, B. L., 2001, Evidence for earthquake induced subsidence about 1100 yr ago in coastal marshes of southern Puget Sound, Washington: Geological Society of America Bulletin, v. 113, p. 1299–1311.

Sherrod, B.L., Blakely, R.J., Weaver C., Kelsey H.M., Barnett E., and Wells R., 2005, Holocene fault scarps and shallow magnetic anomalies along the southern Whidbey Island fault zone near Woodinville, Washington: U.S. Geological Survey. Open File Report, v. 2005-1136, p. 35.

Sherrod, B.L., R. J. Blakely, C.S. Weaver, H.M. Kelsey, E. Barnett, L. Liberty, K.L. Meagher, and K. Pape, 2008, Finding concealed active faults: Extending the southern Whidbey Island fault across the Puget Lowland, Washington: Journal of Geophysical Research, v. 113, B05313, p. 1-25.

Sherrod, B.L., Barnett, E., Schermer, E., Kelsey, H.M., Hughes, J., Foit, F. F., Weaver, C.S., Haugerud, R., and Hyatt, T., 2013, Holocene tectonics and fault reactivation in the foothills of the north Cascade Mountains, Washington: Geosphere, v. 9; p. 827– 852

Taylor, J, 2013, A Gravity Study of Holocene Active Structures in the Puget Lowland of Washington State: [M.S. Thesis], Auburn, Department of Geosciences, Auburn University, 86 p.

Telford, W.M., Geldart, L.P., and Sheriff, R.E., 1990, Applied Geophysics: Second Edition, New York, Cambridge University Press, 759 p.

Wells, R.E., Weaver, C.S., and Blakely, R.J., 1998, Forearc migration in Cascadia and its neotectonic significance: Geology, v. 26, p. 759-762.